3. ANTIPROTON SOURCE PERFORMANCE AND PROJECTIONS*

3.1 Current Performance and Required Improvements

Figure 3.1 shows the general layout of the Antiproton Source. A brief review of antiproton production is given here in order to define terms. A 1.5-μsec-long pulse train of 82 bunches of 120 GeV/c protons is focused to a small spot size on a nickel target. Antiprotons produced over a large spread of angles and energies centered about the forward direction and 8 GeV are collected and focused by a lithium lens into the AP2 beam line. At the end of the AP2 beam line, they are injected into the Debuncher ring, where the antiproton bunches are rotated and adiabatically debunched to form a dc beam. The dc beam is then stochastically cooled in all 3 dimensions by 2-4 GHz systems. The beam is then transferred via the D/A line to the injection orbit of the Accumulator ring. In the Accumulator, each pulse of beam is rf-stacked to the central orbit (the stack tail) and then stochastically stacked in momentum space to the core orbit of the Accumulator. There are 9 separate stochastic cooling systems in the Accumulator: 1-2 GHz stack tail momentum, vertical and horizontal, 2-4 GHz core horizontal, vertical, and momentum, and 4-8 GHz core horizontal, vertical, and momentum systems. (The stack tail horizontal system is currently used for longitudinal cooling.) When a sufficient number of antiprotons has been accumulated in the core (usually 80-200$\times 10^{10}$), stacking is stopped and the core is cooled to as high a density as possible.

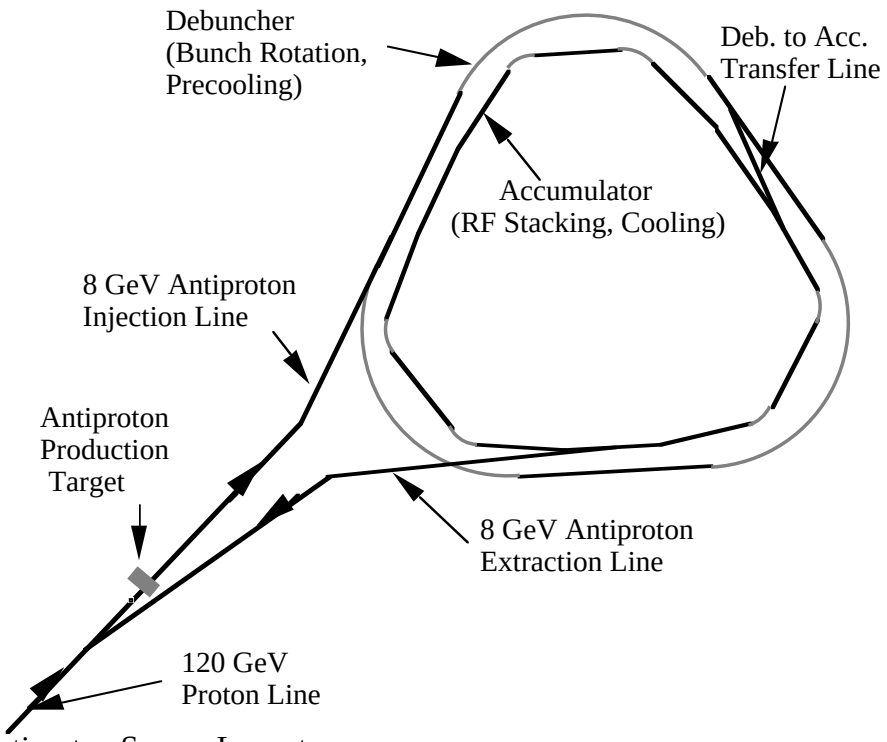

Figure 3.1. Antiproton Source Layout

Beam is then extracted from the Accumulator via the AP3 line and injected into the Main Ring for acceleration and injection into the Tevatron. Typically, 50% of the stack is extracted in six 1.5 eV-sec h=2 bunches. Table 3.1 lists some relevant machine parameters.

* Last revised on August 5, 1998.

Table 3.1. Debuncher and Accumulator parameters

	Accumulator	Debuncher
Central Momentum (MeV/c)	8815.	8883.
Revolution Frequency (MHz)	.628820	.590035
Circumference (meters)	474.4	505.2
Frequency slip factor η	-.023	-.006
Momentum Aperture	2%	4%
Transverse Aperture (π-mm-mrad)	7 - 12	24 - 28
Maximum Dispersion (meters)	10.0	2.1
Maximum β function (meters)	33.	20.
Stochastic Cooling Bands (GHz)	1-2, 2-4, 4-8	2-4

3.1.1 Antiproton Source Performance

During Collider Run 1b the Antiproton Source has been able to stack as much as 7.2×10^{10} antiprotons per hour at small stack sizes ($<50\times10^{10}$) with 3.2×10^{12} protons/pulse incident on the production target every 2.4 seconds. The first column of Table 3.2 shows beam intensities and efficiencies at various stages of the antiproton collection and cooling process for Run 1b. In this table transverse emittances are the 95% real (unnormalized) emittances.

At large stack sizes, the stacking rate drops due to adverse effects of the stack tail cooling system in the Accumulator. Specifically, as the stack core grows the core cooling systems cannot overcome the transverse and longitudinal heating due to the stack tail momentum system. Beam is then lost longitudinally (by rf phase displacement of the stack tail beam back toward the injection orbit) and transversely. This effect is shown in Figure 3.2. The stacking rate does not drop noticeably until the core exceeds about 50×10^{10}. In practice, the stacking rate is optimized by decreasing the pulse repetition rate as the stack core grows. During Collider Run II, the maximum stack size is expected to be $100\text{x}10^{10}$.

In preparation for extracting antiprotons, stacking is stopped and the Accumulator core beam is stochastically cooled in all 3 dimensions as much as possible. Figure 3.3 and Figure 3.4 show transverse emittance and σ_p as a function of stack size just prior to antiproton extraction. All 6 Accumulator core cooling systems are used in this process. For a stack size of 10×10^{10} antiprotons, extrapolated emittances are 0.4π to 0.6π mm-mrad (4π to 6π normalized) and σ_p = 2 to 3 MeV. The transverse emittance is well within the 10π mm-mrad (normalized) and more than 95% lies within the 10 eV-sec specified for transfers to the Recycler. However, the current core cooling systems performance will be degraded by a factor of about 2 with the Accumulator lattice change (the mixing factor is worse by a factor of 2) Furthermore, it should be noted that the emittances quoted are asymptotic emittances obtained an hour or more after stacking has ceased.

Table 3.2. Current and expected Antiproton Source performance under a variety of upgrades

	Run 1b	Run II no upgrades	+ cooling	+ cooling, beam sweep	+ cooling, beam sweep, Li lens upgrade	+ cooling, beam sweep, Li lens upgrade, 25π aperture
upgrade designation			upgrade 1	upgrade 2	upgrade 3	upgrade 4
protons/pulse on target (10^{12})	3.2	5.0	5.0	5.0	5.0	5.0
cycle time (sec)	2.4	1.5	1.5	1.5	1.5	1.5
yield into Deb. ($\bar{p}$ /10^{6} proton)	21.0	17.8	17.8	21.0	22.5	28.1
$\bar{p}$ /pulse into Deb. (10^{7})	6.7	8.9	8.9	10.5	11.2	14.0
$\bar{p}$ /hour into Deb. (10^{10})	10.1	21.4	21.4	25.2	27.7	33.7
initial Deb. emit. (π-mm-mrad)	20.0	20.0	20.0	20.0	20.0	25.0
final Deb. emit. (π-mm-mrad)	4.1	6.9	-	-	-	-
Deb. to Acc. transfer effic.	.80	.60	1.00	1.00	1.00	1.0
$\bar{p}$ /pulse into Acc. (10^{7})	5.4	5.3	8.9	10.5	11.2	14.0
$\bar{p}$ /hour into Acc. (10^{10})	8.1	12.8	21.4	25.2	27.7	33.7
Accumulator stacktail+rf eff.	.90	.90	.90	.90	.90	.90
$\bar{p}$ /hour stacked (10^{10})	7.2	11.5	19.3	22.7	25.0	30.3

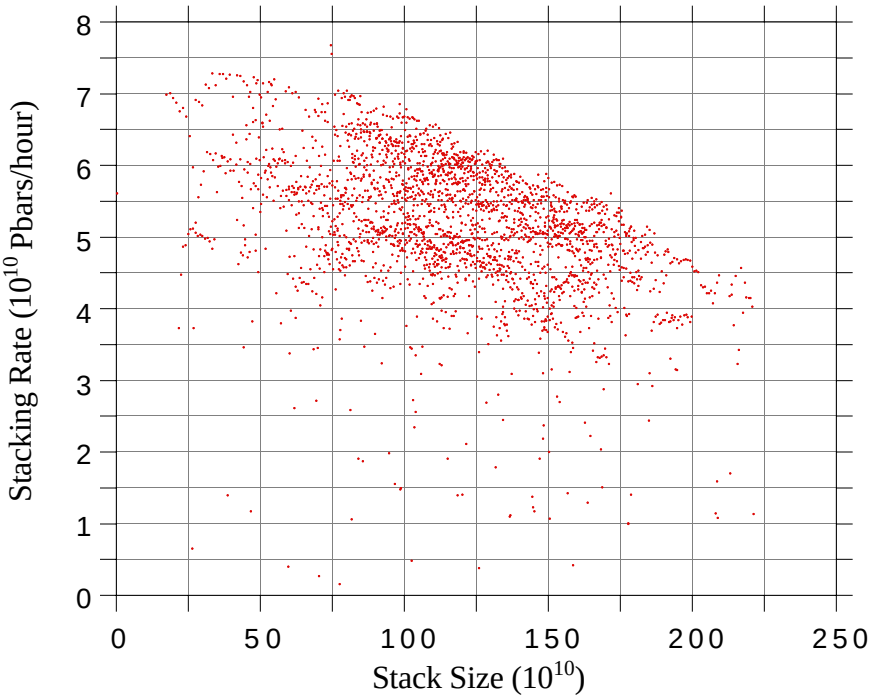

Figure 3.2. Antiproton stacking rate vs. stack size. The data are from April 1995.

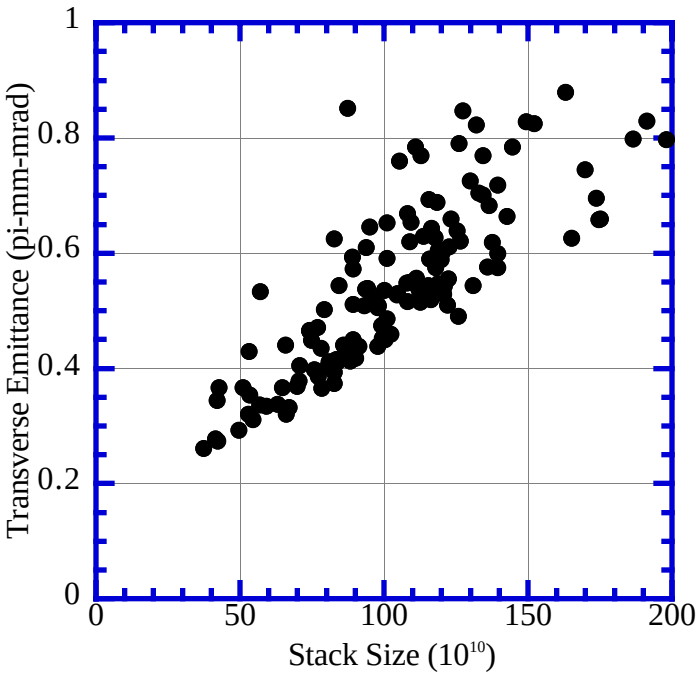

Figure 3.3. Transverse emittance (unnormalized) vs. stack size prior to antiproton extraction.

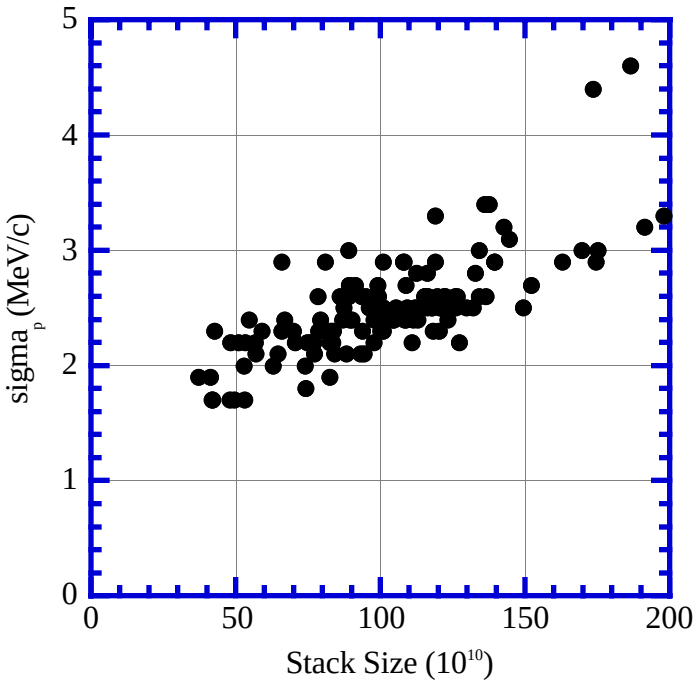

Figure 3.4. Core momentum width vs. stack size prior to antiproton extraction.

3.1.2 Antiproton Source Limitations and Required Improvements

For Run II it is required to stack 20×10^{10}/hour up to stack sizes of 100×10^{10}. At the end of each stacking period (1 to 4 hours) the emittances must be less than 10π-mm-mrad (normalized), and the amount of beam stacked must be contained in a 10 eV-sec longitudinal phase space (about 6 MeV full width). The time allotted for the extraction process 5% of the stacking time (about 5 to 10 min) so as not to compromise the average stacking rate. The major impediments to meeting these requirements are the following:

1) Target and lithium lens survivability: In order to maintain a small spot size on the target, which is necessary for keeping the antiproton yield high, a beam sweeping system will need to be built. This will increase the yield by approximately 18% over the no-beam-sweeping case. This increase is reflected as the second upgrade of Table 3.2. If the lithium lens can be operated reliably at a gradient of 900 T/m, the yield will increase another 17%. This is reflected as upgrade 3 of Table 3.2. These issues are discussed in detail in Section 3.2.

2) Debuncher stochastic cooling: The current system is gain-limited because the stochastic cooling kickers cannot handle the required power and the thermal noise power is large. The Debuncher-to-Accumulator transfer efficiency suffers as a result, and the Accumulator stack tail efficiency also suffers. In addition, the reduced cycle time in Run II will necessitate faster cooling. The proposed upgrades are discussed in Section 3.3. Table 3.2 indicates that the Debuncher cooling upgrade, coupled with other upgrades, should be capable of effectively cooling close to 30×10^{10}/hour.

3) Accumulator stack tail stochastic cooling: Simulations show that the current Accumulator cooling systems will stack $12\text{x}10^{10}$/hour at small stack sizes. An experiment on proton stacking achieved at rate of $12\text{x}10^{10}$/hour.[1] The flux of 8 GeV protons from the target was approximately 3 times the flux of antiprotons. By doubling the bandwidth of the stack tail cooling systems to 2-4

GHz and halving η to -.012, we will increase the stacking rate of the Accumulator to more than 20×10^{10}/hour. These issues are discussed in detail in Section 3.3.3.7.

4) Accumulator core cooling: The core cooling systems are marginal, particularly for frequent transfers to the Recycler. We plan to improve the performance of the 4-8 GHz core cooling systems utilizing R&D work that has been performed in the past few years. These issues are discussed in detail in Section 3.5.

Table 3.2 lists expected antiproton source performance following the various improvements discussed above for Run II. Note that in the absence of any upgrades, the estimated maximum stacking rate is about 11.5×10^{10}/hour.

3.2 Target Station Upgrades

The target station will be upgraded to handle the increased beam flux delivered by the Main Injector. Described below in summary are the status of two new systems (beam sweeping system and proton lens), upgrades to the target SEM and the collection lens, and beam dump/radiation shielding issues.

Figure 3.5 shows a layout of the future upgraded target station. The AP1 beam line transports and focuses the 120-GeV protons from the Main Ring onto the target. Antiprotons produced in the target are collected by a lithium lens and deflected by the pulsed magnet into the AP2 beam line for injection into the Debuncher. The upstream sweep magnets will be installed at the end of the AP1 beam line near the focal point of the proton lens. The downstream sweep magnet will be located between the collection lens and the pulsed magnet, near the focal point of the collection lens.

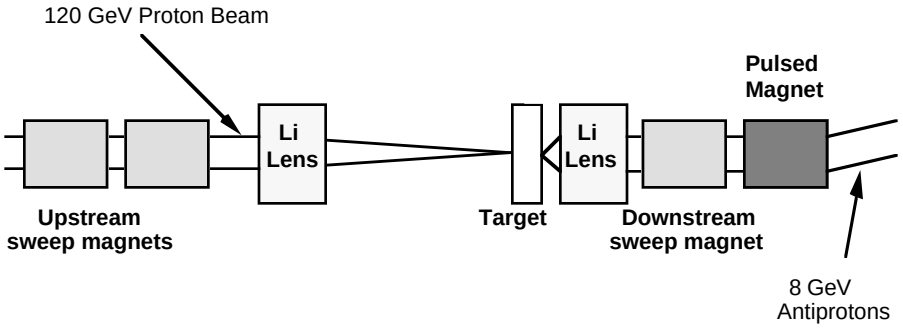

Figure 3.5. Components in the target vault of the upgraded target station. The pre-target SEM and the beam dump are not shown.

3.2.1 Beam Sweeping System.

The efficiency of collecting antiprotons from the target rises as the size of the proton beam spot on the target is reduced. However at the same time the peak energy deposition on target rises. To bring the density of energy deposition within a 0.1 mm (rms) spot size down to currently existing levels, a system to rapidly sweep the beam spot on the target is planned.[2] The calculated dependence of yield on spot size is plotted in Figure 3.6 for a circular beam spot. Also shown in this figure are MARS10 calculations of energy deposition for 5×10^{12} protons per pulse.[3] Estimates of the peak density of energy deposition per pulse achieved to date are about 800 J/g. This is above the melting point of copper (about 600 J/g), and close to the melting point of nickel (about 1000 J/g). Local disintegration of a nickel target has been observed when the target rotation mechanism failed. Less severe damage was observed with a slowly-rotating target.[4] In order to hold peak

energy deposition below damaging levels, the spot size was increased to 0.2 mm after the Linac upgrade, and under Main Injector conditions (5×10^{12} protons in a 1.6 μs pulse), the spot size would have to be increased to at least 0.30 mm. The alternative is to sweep the beam on the target. Reducing the spot size to the smallest attainable size (0.10-0.15 mm) leads to a 15-20% increase in yield.

The beam sweeping system currently under development traces a 0.33-mm-radius circular pattern on the target over the 1.6-μs proton beam pulse. The magnets have a 2-phase, 4-conductor stator excited by two power supplies that deliver 625 kHz sinusoidal current waveforms in quadrature to generate a 625-kHz rotating dipole field. Three identical magnets will be used. A pair of upstream magnets, placed at the downstream end of the AP1 beamline where the toroid M:TOR109 now resides, will sweep the 120-GeV proton beam. A single downstream magnet placed in a double module between the collection lens and the pulsed magnet will redirect the 8 GeV antiprotons exiting the collection lens parallel to the AP2 beamline. The sweeping radius is much smaller than the 2 cm diameter of the lithium collection lens and the aperture of the AP2 beam line. Each magnet is 56 cm long. The deflecting field is 900 G. An air gap is used since the beam is already transported through air from upstream of the target to downstream of the pulsed magnet. A water-cooled molypermalloy pressed-powder magnetic core surrounding the current conductors provides a return path for the magnetic field. Approximately 6 kA will be required in the winding to provide the deflecting field, and the inductive voltage drop will be about 5 kV (peak voltage to ground 2.5 kV). Ionization of the air by the particle shower downstream of the target will increase the conductivity of the air between the conductor plates. Electrical losses through the ionized-air path across the gap reduce the Q of the circuit driving the magnet. Estimates based on CASIM calculations predict that the current drain will be less than 100 A, an acceptable amount. These estimates have been confirmed by measurements of leakage current between two conductors placed parallel to the beam path with a voltage drop of up to 16 kV.

Six power supplies will be required, 4 for the upstream magnet pair, and 2 for the downstream magnet. The prototype power supply is based on a 2-stage magnetic pulse compression circuit. Pulse compression is used because the requirements on a thyratron-based power supply driving a linear circuit are severe, and reliable operation under these conditions is questionable. The solid-state power supply is driven by a single thyristor, and pulse compression is provided by Metglas® cores.

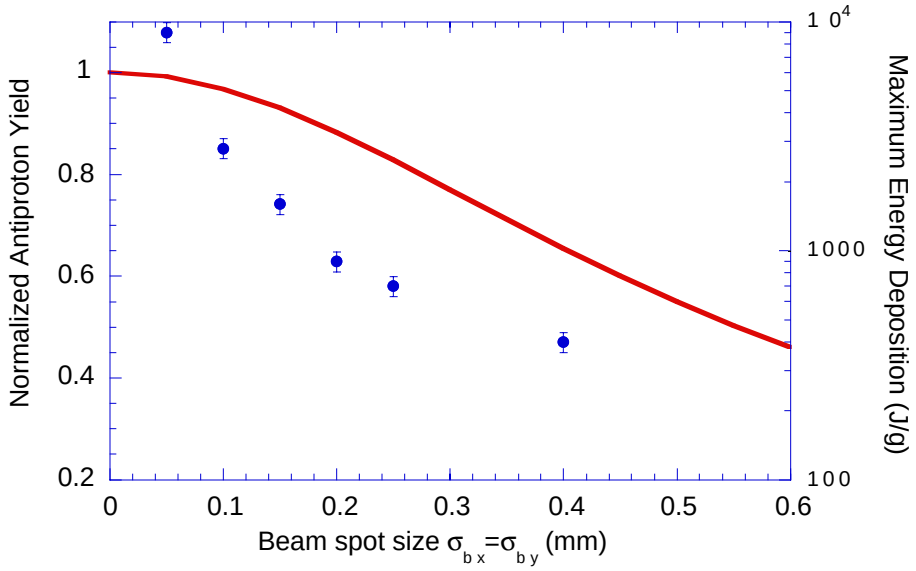

Figure 3.6. Scaling of yield (curve) and peak energy deposition (points) in the target as a function of beam spot size.

3.2.2 Lithium Lens for Proton Beam

A lithium lens has been built to focus the 120 GeV proton beam on the target to a spot size of 0.1 mm.[5] Improved focusing increases antiproton yield and compensates for possible future emittance dilution of the proton beam in the Main Injector. Depending on details of the AP1 proton beam-line tune, we expect that the proton lens, combined with the sweeping system, will improve performance with a 15π mm-mrad (or larger) normalized emittance beam. The projected beam size of the Main Injector proton beam for stacking is about 20π mm-mrad. The lens, with a diameter of 6 mm and length of 8 cm, is expected to operate at a gradient of 2667 T/m and a current of 120 kA. The lens is similar in design to the collection lens. Its main disadvantage is that it absorbs 7.5% of the incident proton beam.

3.2.3 Pre-Target SEM

This SEM, located directly upstream of the target, measures the width and position of the incident proton beam. The titanium wires of the SEM break with less than 3 months of beam exposure at 2×10^{12} protons per cycle. Thus a new module which permits the SEM wires to be removed from the beam during operation has been constructed. When the SEM is placed into position in the path of the beam for measurements, the proton intensity will be temporarily reduced. The new SEM grid has a wire-to-wire spacing of 0.125 mm and will resolve a 0.1 mm beam spot. The SEM is crucial for the commissioning of the proton lens for Run II.

3.2.4 Lithium Collection Lens

The collection lens[6] focuses the antiprotons produced at the target. The current-carrying lithium portion has a diameter of 2 cm and a length of 15 cm. The lithium is encased in a cylindrical water-cooled titanium alloy (type Ti-6Al-4V) pressure vessel. Fermilab lithium lenses of recent design have survived 8 million pulses at a lens gradient of about 740 T/m. Increasing the field gradient of the lens increases the yield. But even a small increase in repetitive stress in the titanium

pressure vessel leads to a much shorter fatigue life of the metal. Thus operation at even 5% greater field gradient has not proven possible beyond 1-2 million pulses. Several improvements in the design of the lens are expected to further improve reliability and field strength. Our goal is reliable operation at 900 T/m although we expect to operate at a lower gradient if we cannot achieve 900 T/m with the reliability of 10 million pulses. At the moment, we do not know how much improvement can be made with the modifications that have been made. Measurements of yield vs. gradient (Figure 3.7) show that 900 T/m will give an 18% increase in yield compared to 740 T/m with the existing AP2 beam-line at a fixed tune. Improvements to the AP2 beam line aperture may raise the antiproton yield at lower gradients while lessening the impact of gradient on yield.

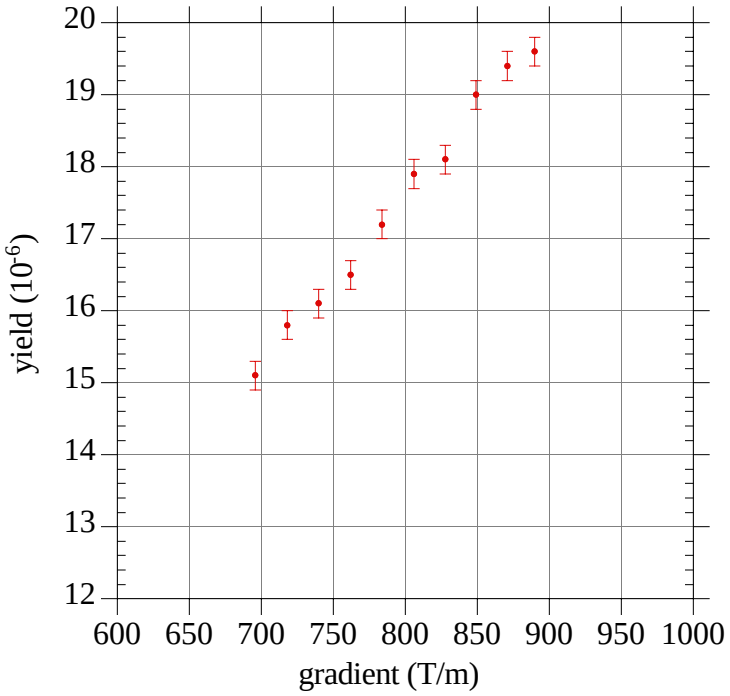

Figure 3.7. Measured yield vs. lithium lens gradient

A number of improvements to the mechanical design have been developed. These improvements include thicker endcaps for the cooling jacket, a stronger beryllium window, and improved handling and placement of welds during construction of the cooling jacket. These improvements have been incorporated into the latest lenses, but have not yet been operated extensively in the target vault. They are expected to enhance lens reliability.

During the filling process, lithium is pumped under pressure into the evacuated titanium vessel. The preload serves to insure that the lithium cylinder maintains its shape at mid-pulse, when significant magnetic pinch forces are present. Lower preload leads to lower operating stresses; a small stress decrease on the titanium cooling jacket should result in a great increase in the life of the lens for a given field gradient. A recent analysis using ANSYS[7] shows that it is possible to lower the preload pressure in the lithium by at least 15%. The original lens design preload ensured that the lithium would maintain its shape on the first pulse when the lithium is at 20˚ C. At steady state, the lens is at 65˚ C and the additional thermal stress on the titanium is approximately the same as the stress due to preload. Thus, at steady state almost no preload is needed. If one could reduce the lithium preload from 2300 psi to 500 psi, then the lens would be able to operate at 1000 T/m

without deformation of the lithium cylinder. Lenses with preload as low as 1500 psi have been built for Run II.

Gaseous products from the $^{6}Li(n,\alpha)^{3}H$ reaction between ^{6}Li in natural lithium and thermal neutrons are expected to build up over time, possibly affecting the operation of the lens.[8] Swelling of the lens is expected, due to the pressure of the contained gas, potentially limiting the lifetime of the lens under an intense beam environment. To avoid this problem, we have identified a source of 99% isotopically pure ^{7}Li. Collection lenses for Main Injector operation will be built using this material.

3.2.5 Single-Turn Pulsed Magnet

The single-turn pulsed magnet has survived more than 25 million pulses at proton intensities between 1.5 and 3.3×10^{12} protons per pulse. It is expected that no changes will be required for Main Injector operation.

3.2.6 Beam Dump

The Antiproton Source beam dump now absorbs 25 kW of beam power. A capacity of 56 kW is needed for Main Injector conditions. Since we are only using half of the available cooling channels, we can easily double the cooling capacity of the existing system. We plan to use all the channels for Run II. We can also increase the flow rate through the channels, but it should not be necessary.

3.2.7 Radiation Safety Issues

Since 1990, both the target vault shielding and the target air system have been upgraded. Under Main Injector conditions, the radiation level on the roof of the AP0 service building is expected to be less than 50 mR/hr. Posting a High Radiation Area sign on the fence around the ladder leading to the roof of the AP0 service building will be sufficient for Run II. No other shielding changes will be needed in or around the AP0 service building.

The existing air system keeps the portion of AP0 that can be occupied by personnel at a positive pressure with respect to the outside, the vault and both adjoining beam lines. A HEPA filter in the AP1 beamline removes dust from the air(some of which is radioactive). The flow is controlled in such a way that airborne radionuclides have two hours to decay in the tunnel enclosure before exiting. This is deemed to be sufficient for all radionuclides which could arise from proton-nickel interactions.

The 1991 Antiproton Source Radiation Shielding Assessment document presently limits the number of protons on target to 5.4E15 protons per hour. This is only 2.25 protons per pulse for a 1.5 second duty cycle. This document must be updated to reflect the Main Injector goal of 5E12 protons per pulse at a 1.5 second repetition rate.

3.2.8 Injection Line Transverse Aperture Increase

Using reverse protons, the transverse aperture of the Debuncher antiproton injection line (AP2) has been recently measured to be about 20π x 20π mm-mrad for particles centered in the momentum aperture ($\delta p/p=0$). The aperture limitation is in the downstream end of the beam line, which involves a vertical bend downward by a dipole magnet, a vertical bend upward by the off-center traversal of a large Debuncher quadrupole, followed by vertical kicks by a septum magnet and fast kicker magnet. Detailed examination of the beam pipe in this area verifies that the maximum attainable transverse aperture is about 20π x 20π mm-mrad. We have started a program to increase the AP2 aperture to nominally 40π x 40π mm-mrad, with the eventual goal of attaining

a real aperture of 32π x 32π mm-mrad for particles at δp/p=0. The transverse aperture of the Debuncher itself has physical apertures which are typically 40π x 40π mm-mrad or larger, but the Debuncher acceptance is measured to be about 28π x 24π mm-mrad at δp/p=0.

The following upgrades are underway or being planned for the downstream end of AP2:

1. Minor beam pipe modifications near D4Q4 to increase the vertical aperture for injected beam to 40π;
2. Addition of a motorized stand to the Debuncher quadrupole D4Q8 to allow independent horizontal and vertical position and angle control of the closed orbit in the vicinity of the injection region;
3. Design of a new injection septum magnet, similar to the original one, but with a 10% larger horizontal aperture;
4. Modification to the Debuncher large quad used to bend the injected beam upward to allow for a 10% larger horizontal aperture beam pipe.

Upgrades 1 and 2 above will increase the downstream AP2 vertical aperture to 40π mm-mrad, while upgrades 3 and 4 will increase the horizontal aperture to 40π mm-mrad. The upstream end of AP2 is nominally 40π x 40π mm-mrad, but beam studies will be required to understand optimum beam steering. In addition, beam studies will be required to understand the current limitations in the Debuncher transverse aperture if the full 32π mm-mrad aperture is to be realized. Table 3.3 shows projected antiproton yield increases under various upgrade scenarios. This table is based on Monte Carlo calculations and assumes a proton beam size of .15 mm RMS on the production target and a beam line tuned to optimize yield into the Debuncher.

Table 3.3. Antiproton yield into the Debuncher as a function of lithium lens gradient and downstream transverse aperture. Also listed are the beta function at the downstream lens focus, target thickness, and target-to-lens distance which optimize yield into the Debuncher. Yields are normalized to Run I operating conditions.

	yield (/10^6 protons on target)	β at ds lens focus (m)	target thickness (cm)	target center to lens face (cm)
20π, 740 T/m	21.0	4.5	6.5	21.2
25π, 740 T/m	25.6	4.3	6.5	21.2
32π, 740 T/m	30.0	3.9	6.5	21.2
20π, 900 T/m	22.5	4.3	6.0	17.0
25π, 900 T/m	28.1	3.9	6.0	17.0
32π, 900 T/m	34.1	3.7	6.0	17.0

3.3 Debuncher Stochastic Cooling

3.3.1 Performance of the existing 2-4 GHz system

Each pulse of beam is cooled in all 3 dimensions in the Debuncher during the entire production cycle. There are 128 LN_2 cooled pickup pairs and 128 kicker pairs for each transverse system. Momentum cooling is done by the "filter method" using the sum mode signals from the transverse electrodes, and notch filters are additionally used in the transverse systems to minimize thermal noise power. All 3 systems now operate in the 2-4 GHz frequency range.[9] After bunch rotation, the momentum width (95% full width) is cooled from 0.30% to 0.17%. The transverse emittances are cooled from 16-17 π mm-mrad to 3-4 π mm-mrad (unnormalized 95% emittances). The

momentum width is inferred from the frequency width of the longitudinal Schottky spectrum. The transverse emittance at the beginning of the cycle is determined by measuring yield as a function of transverse scraper position, and the transverse emittance at the end of the cycle is determined by measuring the beam transverse dimensions with SEM's in the D/A line. In addition, the transverse emittance measurements are corroborated by measurements of the time evolution of the power in the transverse Schottky bands during the cooling cycle (Figure 3.8).

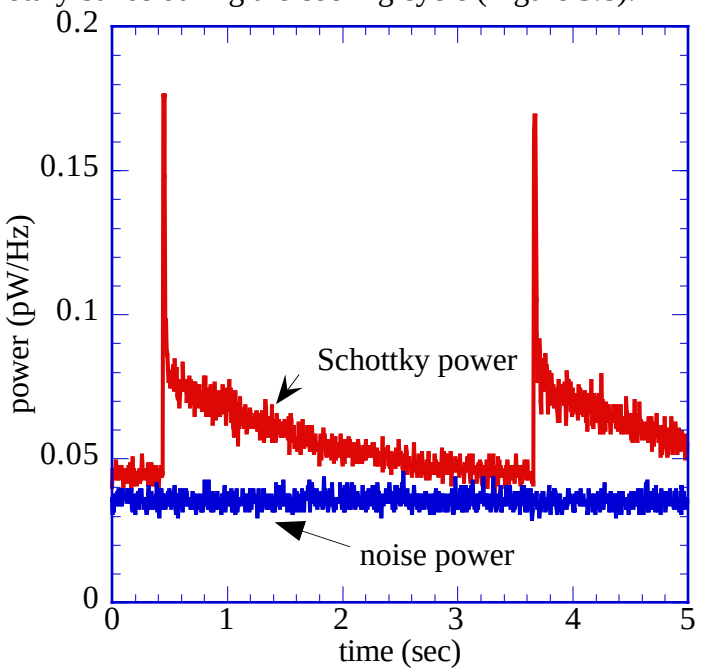

Figure 3.8. Power in a vertical Schottky band as a function of time during the cooling cycle. This power (minus noise power) is proportional to transverse emittance.

The transverse emittance cooling rate is given by[10]

$$-\frac{1}{\varepsilon_\perp}\frac{d\varepsilon_\perp}{dt} = F_0 \sum_l \left\{ g_l T_l - \frac{N}{2}\left| g_l T_l \right|^2 \left(M_l + U_l \right) \right\} \qquad [3.1]$$

where for simplicity we have neglected imaginary parts due to "bad mixing", non-optimum pickup to kicker betatron phase advance, and microwave signal processing hardware. The summation is over Schottky bands and the quantities within the summation are averaged over beam frequencies in each Schottky band. In the above equation:

$g_l = \frac{\sqrt{\beta_{PU}\beta_K}}{2} \cdot \frac{eF_0}{\beta^2 E} \cdot Z'_{PU} \cdot g_{E,l} \cdot K_\perp$ is the gain function;[11]

$M_l = \frac{1}{l\eta\sqrt{\pi}\,\frac{\Delta p_{95\%}}{p}}$ is the average mixing factor for a Gaussian beam distribution;

$T_l = \frac{1}{1 - S(\omega_l)}$ is the shielding factor, where $S(\omega_l) = \frac{-iF_0 N}{2}\int \frac{g_l(\omega)\Psi(\omega)d\omega}{\omega - \omega_l}$ and

$T_l \to \frac{1}{1 + \frac{N g_l M_l}{\sqrt{2}}}$ at the center of a Gaussian beam;

$U_l =$ (thermal noise power density)/(average Schottky power density).

where F_0 is the revolution frequency, β_{PU} and β_K are the beta functions at the pickup and kicker, and Z_{PU} is the pickup (and kicker) impedance. M_l is determined by measuring the longitudinal Schottky width during the cooling cycle, T_l is determined by measuring the signal suppression effect, g_l can be determined from M_l and T_l, and U_l can be directly measured by comparing the Schottky spectrum with and without beam. These quantities can then be inserted into the basic cooling equation above, and the time evolution of the emittances calculated and compared to the measured emittance cooling rate. The result is shown in Figure 3.9.

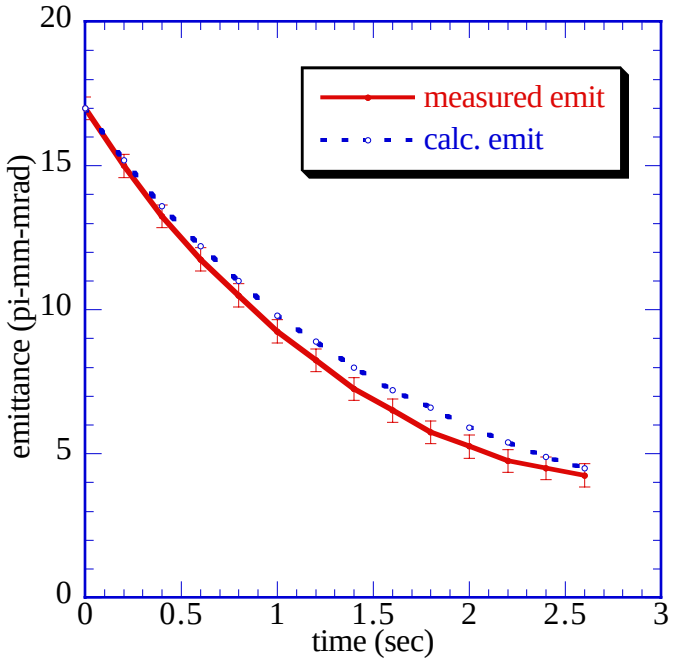

Figure 3.9. Comparison of the calculated and measured evolution of transverse emittance under Run 1b conditions. The observed cooling rate is slightly faster than the calculated rate.

At mid-band M_l is 6 at the beginning of the cycle, increasing to 11 at the end of the cycle; U_l is 10 at the beginning of the cycle, increasing to 40 at the end of the cycle. Optimum gain at the center of the beam distribution is given by

$$g_{opt,l} = \frac{1}{\frac{M_{peak,l}}{2} + U_l}. \qquad [3.2]$$

The system operates substantially below the optimum gain. In addition, the maximum cooling rate is limited by the thermal power (U_l). We are prevented from increasing the gain by the power limitation of the kicker tanks -- these tanks are limited to about 1200 W per system by the power handling capability of the terminating resistors, solder joints, vacuum feedthroughs, and microwave hybrids. (At 1200W 95% of the power at the kickers is thermal power.)

3.3.2 Overview of the new 4-8 GHz cooling systems

During Run II the cycle time will be 2.4/1.5 = 1.6 times faster, and the intensity per pulse will be about 5.0/3.2 = 1.6 times greater than in Run 1b. An improvement in the Debuncher cooling is required to meet the demands of Run II. It is possible to meet these demands with improvements to

the 2-4 GHz system. However, we have chosen to increase the bandwidth to 4-8 GHz so that we will be able to accommodate antiproton fluxes beyond those anticipated in the initial stages of Run II.

The most critical task is to develop 4-8 GHz pickup and kicker electrodes. The 4-8 GHz band will be spanned by 8 narrow band pickups and 4 narrow band kickers. The pickups and kickers are based on a new design[12] that was tested[13] in 1997. This narrow-band approach is similar in concept to the one used at CERN.[14]

The pickups will be cooled to less than 10 ˚K by replacing the LN cryogenics (80 ˚K) with liquid helium. The pickup signals will be amplified by commercial cryogenically cooled amplifiers. The 8 pickup bands then be combined pair-wise into the 4 kicker bands and the signal will be transmitted across the ring using coaxial cable. It is unnecessary to use optical techniques (see section 3.4.4.4) because of the low bandwidths involved.

The four kicker bands will be implemented with 16 TWT's driving 16 kicker electrodes, namely 4 TWT/kicker pairs per band. The rated power of the system is 1600 W. A critical feature of the kicker design is the ability of the structure to dissipate 100 W at high vacuum. A schematic of the system is shown in Figure 3.10.

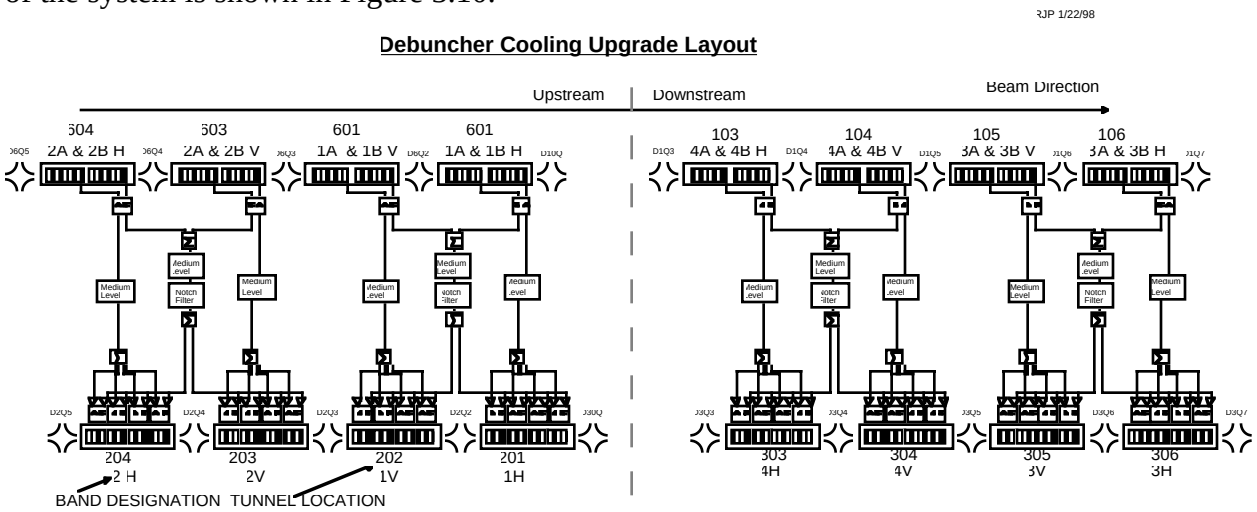

Notes: 12 total cooling systems. Eight narrow bands on pickup end. Two bands combined to make four trunks for each of the Horizontal, Vertical and Longitudinal cooling. The Kickers utilize wider bands consisting of the addition of two pickup bands. The signals are summed externally after the cryo amplifier. The momentum signal is combined from one H and one V system in each band. Bands are located in the lattice so as to take advantage of beam size.

Band Designation	Frequency GHz	Span GHz
1A	3.89-4.64	0.75
1B	4.47-5.21	0.74
1	3.89-5.21	1.32
2A	5.01-5.72	0.71
2B	5.57-6.24	0.67
2	5.01-6.24	1.23
3A	6.10-6.73	0.63
3B	6.60-7.20	0.60
3	6.10-7.20	1.10
4A	7.05-7.64	0.59
4B	7.46-8.11	0.65
4	7.05-8.11	1.06

Figure 3.10. Layout of the 4-8 GHz Debuncher cooling systems. Momentum, horizontal, and vertical cooling systems are shown.

3.3.3 Simulations

3.3.3.1 Assumptions

The basic beam parameters are shown in Table 3.4. The beam size is assumed to be 25π mm–mrad (consistent with current estimates) although we hope to have 30π mm-mrad beams in Run II. The pickup apertures are assumed to be 40π mm-mrad—rather large for a 25π mm-mrad

beam. The momentum changes as momentum cooling proceeds. The calculations are done with a fixed momentum spread corresponding roughly to that obtained at the end of momentum cooling.

Table 3.4. Beam Parameters

Energy spread (full)	18	MeV
Beam Energy	8938	MeV
Initial Beam Emittance	25	π mm-mrad
Accumulator Acceptance	5	π mm-mrad
$\eta = 1/\gamma_t^2 - 1/\gamma^2$	0.006	
Number of particles (Run II)	1×10^8	
Number of particles (TeV33)	4×10^8	

We plan to use an entirely new 4-8 GHz system using 4 relatively narrow bands. This approach was used at the CERN AC. The parameters of the proposed 4-8 GHz Horizontal system are shown in Table 3.5. The Vertical system is identical except the pickup and kicker impedances are slightly different because of small differences in the lattice functions. The impedances were calculated by Dave McGinnis[15] and are consistent with the recently measured sensitivity.[16] The simulations include a more conservative 3 dB loss at the pickup and kicker, not the 1 dB loss specified in Table 3.5.

Table 3.5. 4-8 GHz Horizontal system parameters

PU/Kicker Impedance (peak)	3620	Ω
PU's/Kickers per band	8	
Number of Bands	4	
Combiner Loss	1	dB
Splitter Loss	1	dB
Amplifier Noise Temperature	25	°K
Resistor Temperature	10	°K
PU/Kicker Aperture	40	π mm-mrad
Gain (typical)	147	dB
Power	400	W/band

3.3.3.2 System Gain

The definition of the system gain G per Schottky band is

$$\frac{dA^2}{dt} = 2 f_0 G A^2 \qquad [3.3]$$

where A is the betatron amplitude and $2G$ is the cooling rate for a particular Schottky band. A plot of system gain versus frequency is shown in Figure 3.11. The variations in gain are large and are entirely due to the variations in pickup and kicker sensitivity.

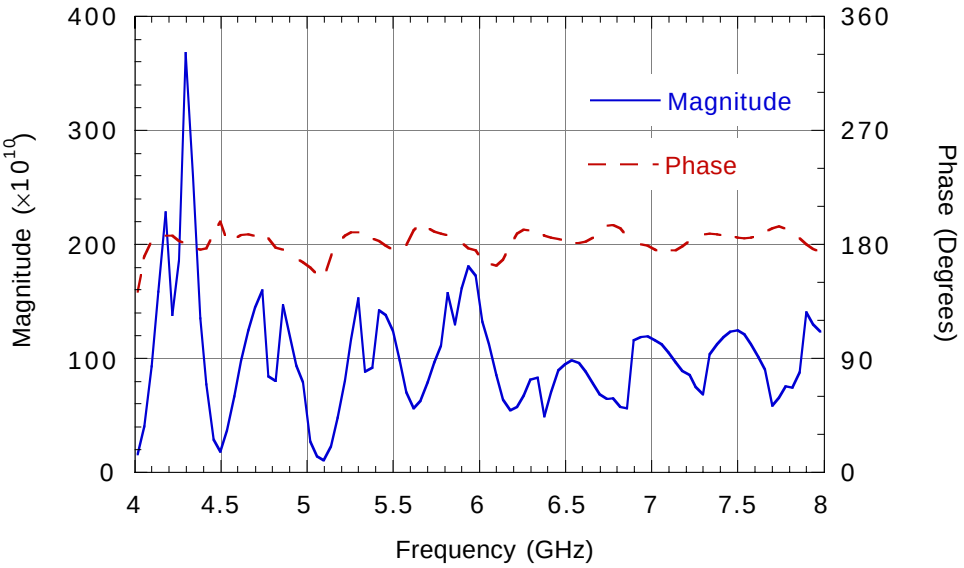

Figure 3.11. Cooling system gain. The gain response is dominated by the pickup and kicker response.

3.3.3.3 Mixing Factor

The mixing factor for the 4-8 GHz system is shown in Figure 3.12. The mixing factor depends only on the lattice parameters and the frequency.

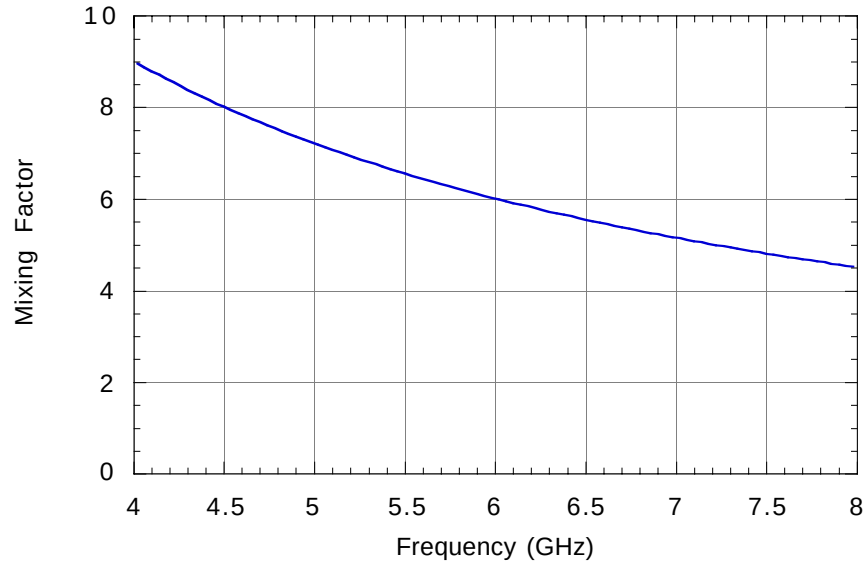

Figure 3.12. Mixing Factor.

3.3.3.4 Signal to Noise Ratio

The signal to noise ratio is shown in Figure 3.13. The large variations come from variations in the pickup sensitivity. It has been assumed that sharp transversal filters are to filter unwanted broad-band noise outside the pickup bandwidth.[17]

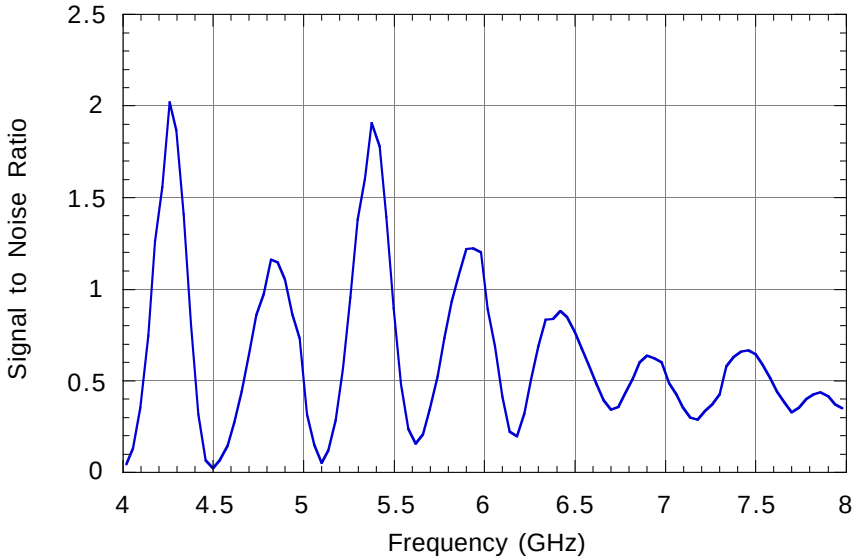

Figure 3.13. Signal to noise ratio.

3.3.3.5 Signal Suppression

Signal suppression is a measure of the strength of the feedback. The signal suppression factor is (1-*GF*), and is equal to 2 at the optimum gain. The factor *GF* is plotted in Figure 3.14 for the 4-8 GHz Horizontal system.

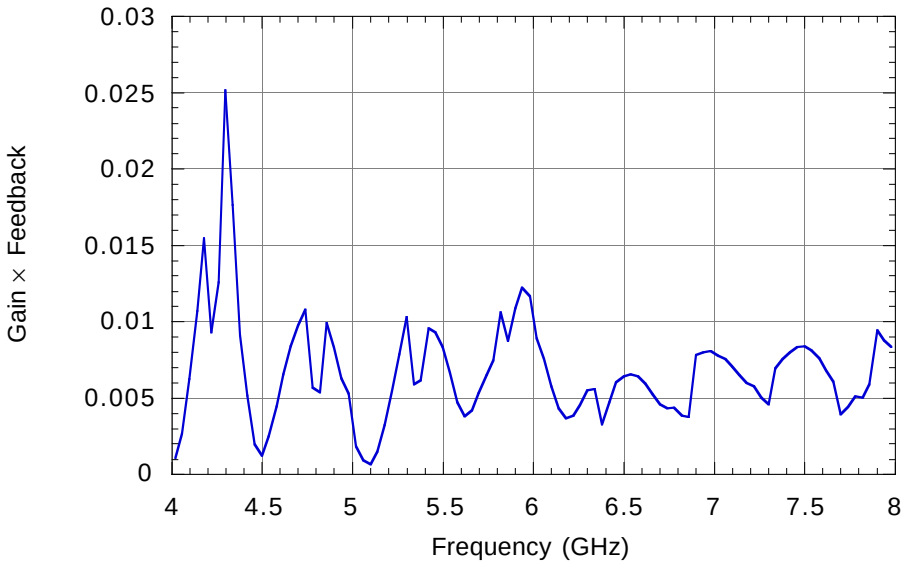

Figure 3.14. Signal suppression factor.

3.3.3.6 Performance in Run II

The performance predicted in Run II under the previously stated assumptions is shown in Figure 3.15, which shows the horizontal emittance versus time. Similarly, Figure 3.16 shows the vertical emittance versus time. The system bandwidths and sensitivities are not finalized, but at this point the vertical cooling system performs noticeably better.. The nominal cycle time is 1.5 sec. The four-band 4-8 GHz system outperforms the 2-4 GHz system. The 2-4 GHz system performs somewhere between 2 and 3 bands of the 4-8 GHz system.

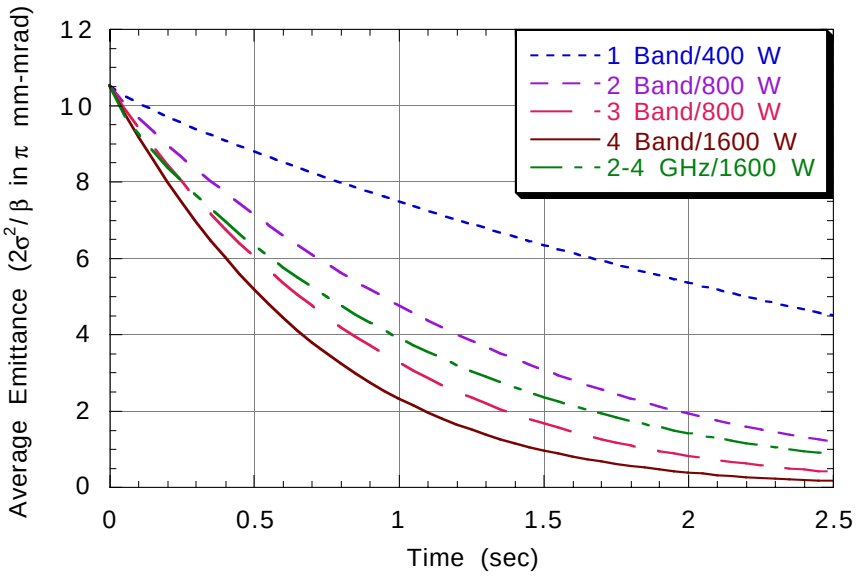

Figure 3.15. The horizontal emittance versus time for the various scenarios.

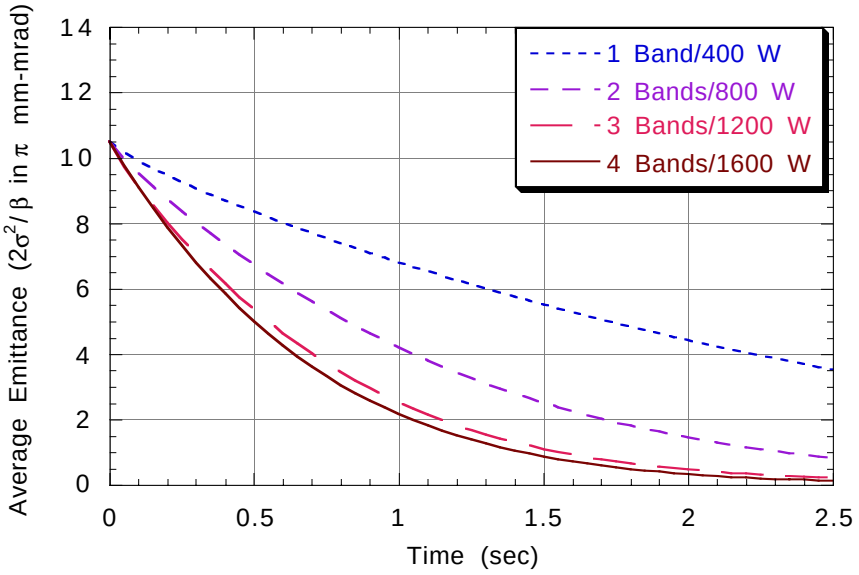

Figure 3.16. The vertical emittance versus time for the various scenarios.

The transfer efficiency is computed as the fraction of beam less than 5π mm-mrad horizontally times the fraction of beam less than 5π mm-mrad vertically. The combination of the data from Figure 3.15 and Figure 3.16 (assuming the 2-4 GHz cooling to be the same in each plane) is shown in Figure 3.17.

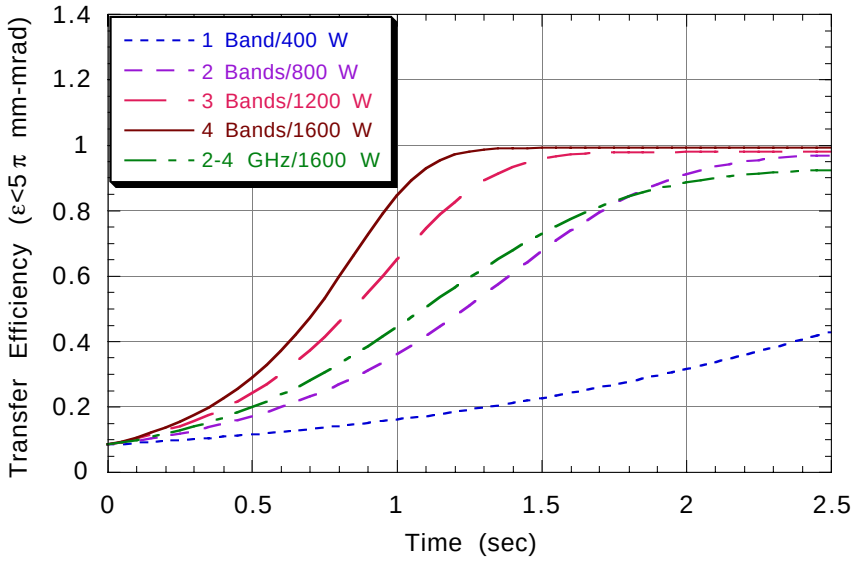

Figure 3.17. Transfer efficiency as a function of time for the various scenarios.

3.3.3.7 Performance with TeV33 parameters

We have also examined the system performance at higher intensity (TeV33 parameters). The results are shown in Figure 3.18 and Figure 3.19. The transfer efficiencies are obtained from the square of the fraction of the beam with a horizontal emittance less than 5π mm-mrad. Since the cooling is less effective in the horizontal plane, the transfer efficiency is probably underestimated. The 2-4 GHz system performance is limited primarily because of its lower bandwidth. The larger particle losses incurred with this system and shown in Figure 3.20 are indicative of the need for more bandwidth.

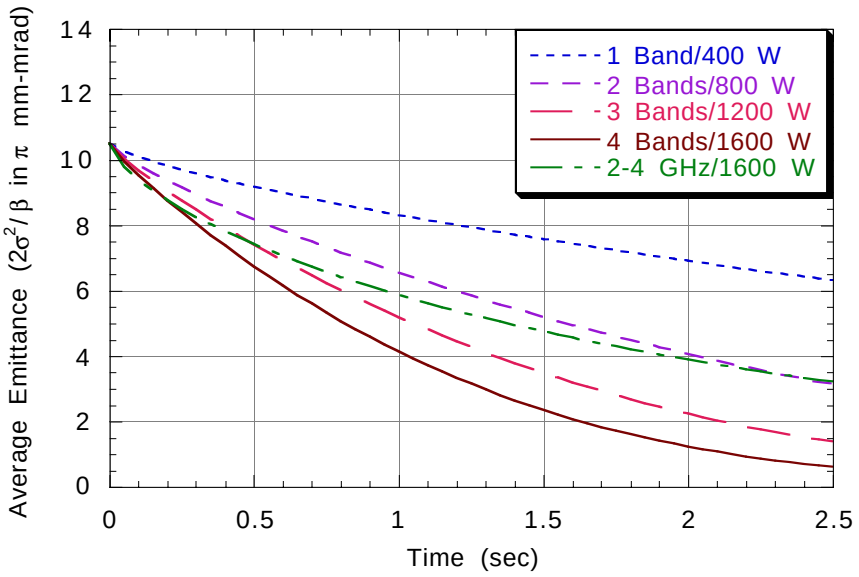

Figure 3.18. Horizontal emittance versus time for Tev33 intensities.

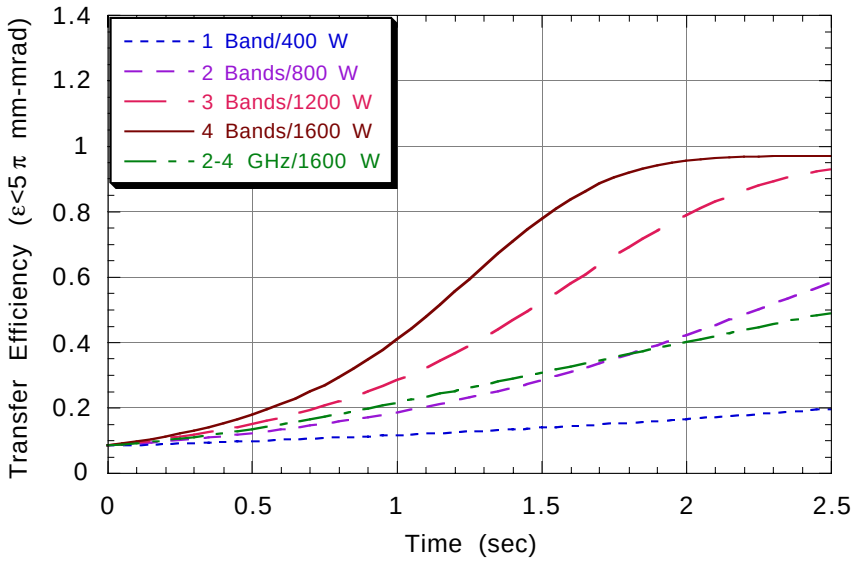

Figure 3.19. Transfer efficiency versus cooling time for TeV33 intensities. The transfer efficiencies are obtained from the square of the fraction of the beam with a horizontal emittance less than 5π mm-mrad.

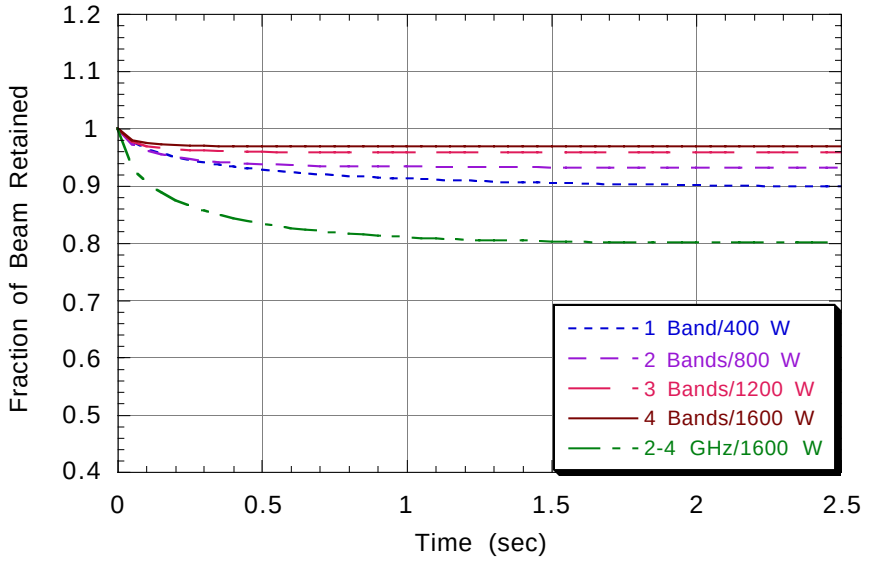

Figure 3.20. Fraction of beam retained as a function of cooling time. The limited bandwidth and relatively high gain of the 2-4 GHz system result in significant particle losses at the beginning of the cycle.

3.4 Stack-Tail System Upgrade

3.4.1 Overview

The beam parameters in the Accumulator will change in the following ways from Collider Run Ib to Run II:

1) The antiproton flux will increase from 2.0×10^7 (peak) to 5.6×10^7 (average) per second. These fluxes correspond to 7.2 mA/hour (peak) and 20 mA/hour (average) respectively;

2) Beam transfers from the Accumulator to the Recycler will take place every 1 to 4 hours.

3) The maximum antiproton stack size will be reduced from 200×10^{10} to 100×10^{10};

The current stack tail cooling system in the Accumulator is inadequate to cope with the increased flux. It is proposed to increase the bandwidth of the stack tail cooling system from 1-2 GHz to 2-4 GHz and to decrease η by a factor of two from -.023 to -.012. The bandwidth change will supply the necessary cooling force to handle the increased flux. The η change will avoid Schottky band overlap, which causes excessive beam heating, and will allow the use of conventional notch filters for gain shaping. In general aspects, the system will be similar to the current system.

The maximum attainable flux in a "perfect" stacking system having a bandwidth of a single octave is given by[18]

$$\phi_{\max} = \frac{1.4 W^2 E_d |\eta|}{p F_0} \text{ sec}^{-1}, \qquad [3.4]$$

where W is the bandwidth, $1/E_d$ is the slope of the exponential gain profile, p is the beam momentum, and F_0 is the revolution frequency. This equation neglects thermal noise, signal suppression, phase variations across the Schottky band, and the effects of periodic beam injection, but indicates that doubling the bandwidth and halving η will double the maximum attainable flux.

E_d is 10 MeV, so that we have for the current stack tail system ϕ_{max} = 21x10^{10}/hour. In addition to the factors mentioned above, other effects that will further reduce the stacking rate are intrabeam scattering, intermodulation distortion in TWT's, realistic gain and phase variations across the microwave band, and cross-talk from transverse cooling systems. We have attempted to include all of these effects (albeit crudely in some cases) so that the current performance of the Accumulator cooling systems is well predicted by the stochastic cooling simulation.

3.4.2 Lattice Modifications

Using the Methodical Accelerator Design (MAD) simulation code, a strategy for raising γ_t in the Accumulator ring and hence lowering η has been developed. The Accumulator is divided into 6 sectors, each containing fourteen quadrupole magnets.[19] The symmetry is three-fold, each of the six sectors being a reflection of the adjacent sector. Within each sector, nine of the quadrupoles are of the small TEV I variety and five are large TEV I quadrupoles. Changes to the quadrupole operation that will enable γ_t to be raised from 5.41 to 6.58, correspondi ng to an η	261.6			261.6	
		3.25			

Q2	-QT	0.9900	264.2	261.6	
Q3	QT	0.9009	264.2	238.0	23.6
Q4	QF	0.9865	231.6	228.5	
Q5	QD	0.9908	234.3	232.0	
Q6	QF	1.1043	231.6	255.8	
Q7	QD	0.9908	234.3	232.0	
Q8	QF	0.9816	231.6	227.3	1.2
Q9	QD	0.9908	234.3	232.0	
Q10	.45724*LQ	0.9900	1294.3	1281.4	32.6
Q11	LQ	0.9900	1294.3	1281.4	32.6
Q12	-LQ	1.0152	1294.3	1314.0	
Q13	-LQ	1.0152	1294.3	1314.0	
Q14	LQ	1.0890	1294.3	1314.0	
Note that column 3 above includes the quad bus changes below.					
QT	10.3809T/m	.9900	264.3	261.6	
QF	9.66333T/m	.9816	231.6	228.5	3.5
QD	9.74126T/m	.9908	234.3	232.0	
LQ	8.93989T/m	.9900	1294.3	1314.0	

Since the current in Q6 will be significantly different from that of the other small quadrupoles, a separate power supply will be required for these 6 quadrupoles. Table 3.7 shows critical lattice parameters for the current lattice and the γ_t upgrade. The tunes remain at 6.609 (horizontal) and 8.607 (vertical), and the phase advance from pickup to kicker in the core and stack tail betatron systems remains close to $\pi/2$. The natural chromaticities in each plane (ξ_x = -11.2 and ξ_y = -13.0) are correctable by decreasing the current in one of the sextupoles in each sector. The dispersion is similar to that of the present Accumulator, with a slightly more negative dispersion in non-critical parts of the ring to accomplish the change in γ_t. The beta functions and dispersion function are shown in Figure 3.21 through Figure 3.23. The physical aperture and beam envelope functions are shown in Figure 3.24 through Figure 3.26.

Table 3.7. Lattice parameters for TEV I design and γ_t upgrade

Lattice Parameter	**TeV I Design**	**γ_t Upgrade**
Maximum β_x (m)	33.23	71.15
Minimum β_y (m)	30.87	31.49
β_x @ high D_x (m)	7.58	2.60
β_y @ high D_x (m)	7.51	6.76
β_x @ low D_x (m)	7.56	10.03
β_y @ low D_x (m)	7.27	4.97
γ_t	5.41	6.58
η	-.023	-.0119
$\Delta\phi$PU-K Core H	9.16π/2	9.08π/2
$\Delta\phi$PU-K Core V	11.00π/2	10.82π/2
$\Delta\phi$PU-K Stack tail H	8.89π/2	8.95π/2

$\Delta\phi$PU-K Stack tail V	11.20π/2	11.16π/2

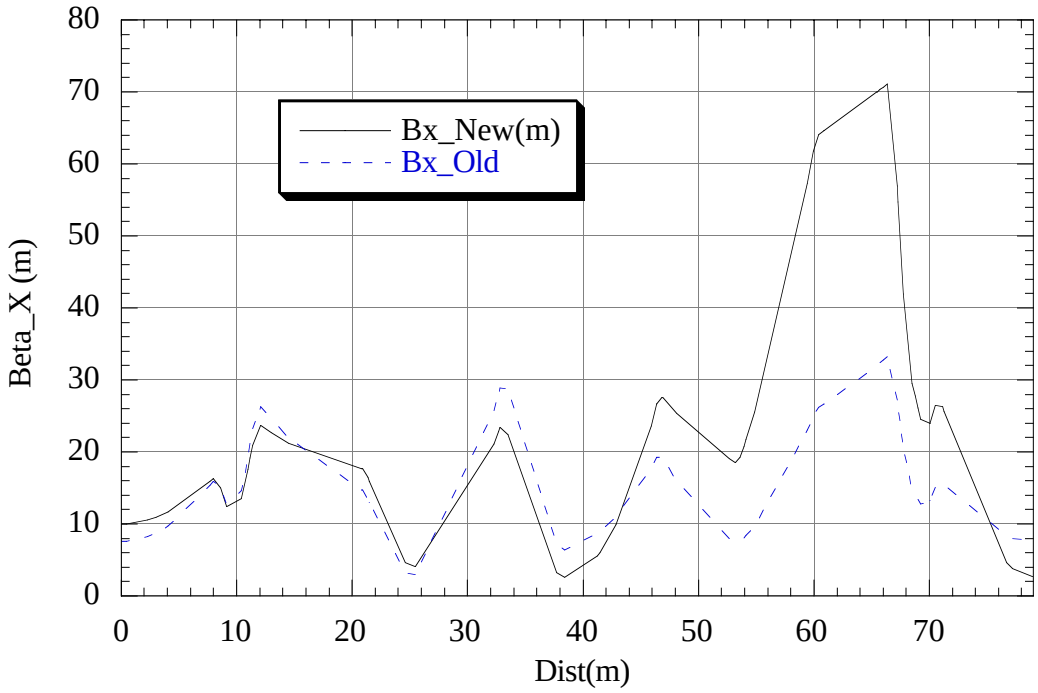

Figure 3.21. Horizontal beta function in one sector (1/6th) of Accumulator.

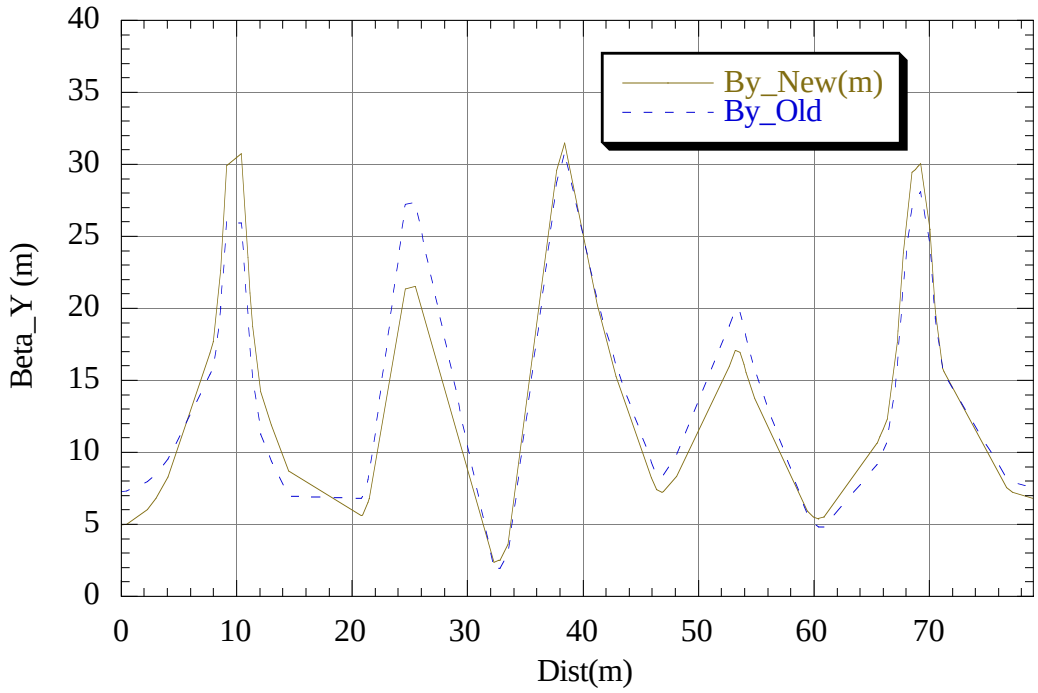

Figure 3.22. Vertical beta function in one sector (1/6th) of Accumulator.

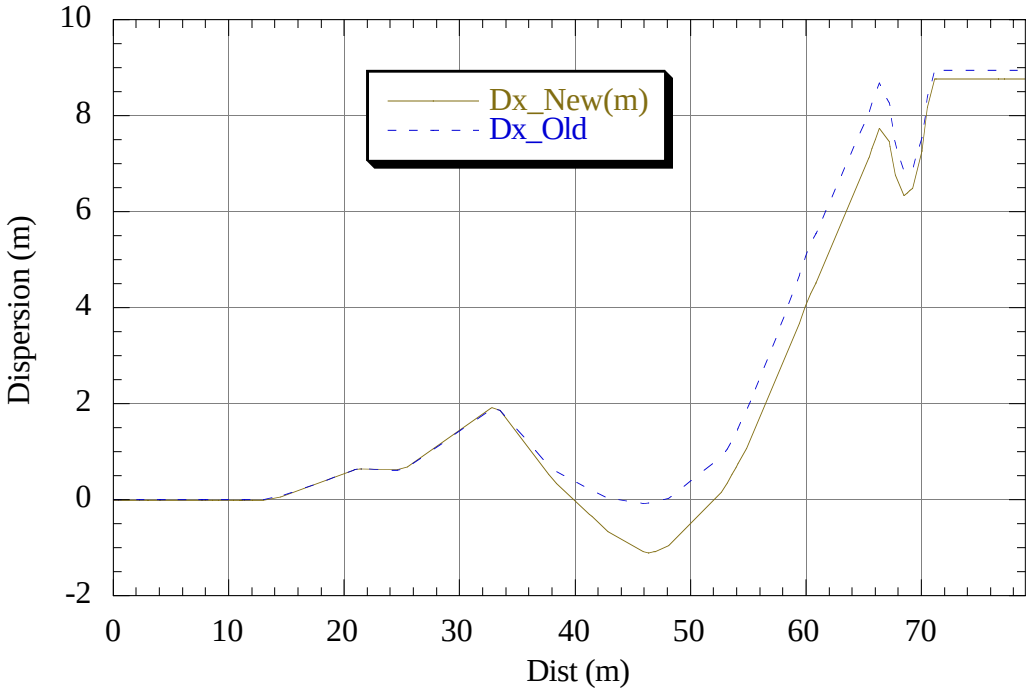

Figure 3.23. Horizontal dispersion function in one sector (1/6th) of Accumulator

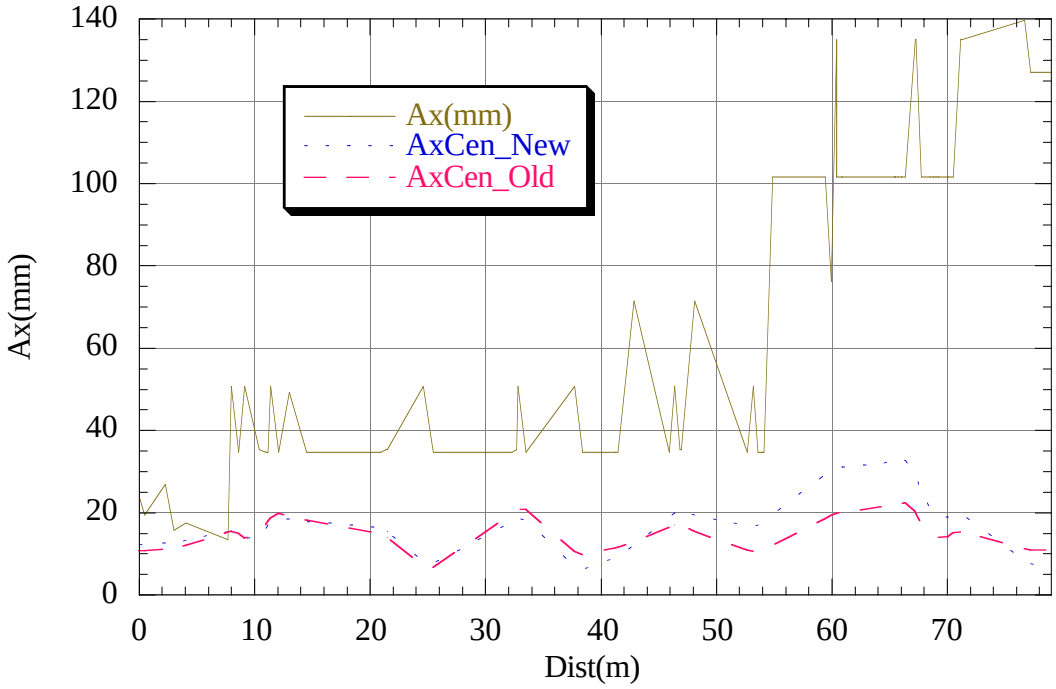

Figure 3.24. Horizontal aperture and beam envelope on the central orbit in one sector (1/6th) of Accumulator; the formula used for the beam envelope is $A_x = \sqrt{\varepsilon\beta/\pi}$ where ε = 15π mm-mrad (unnormalized).

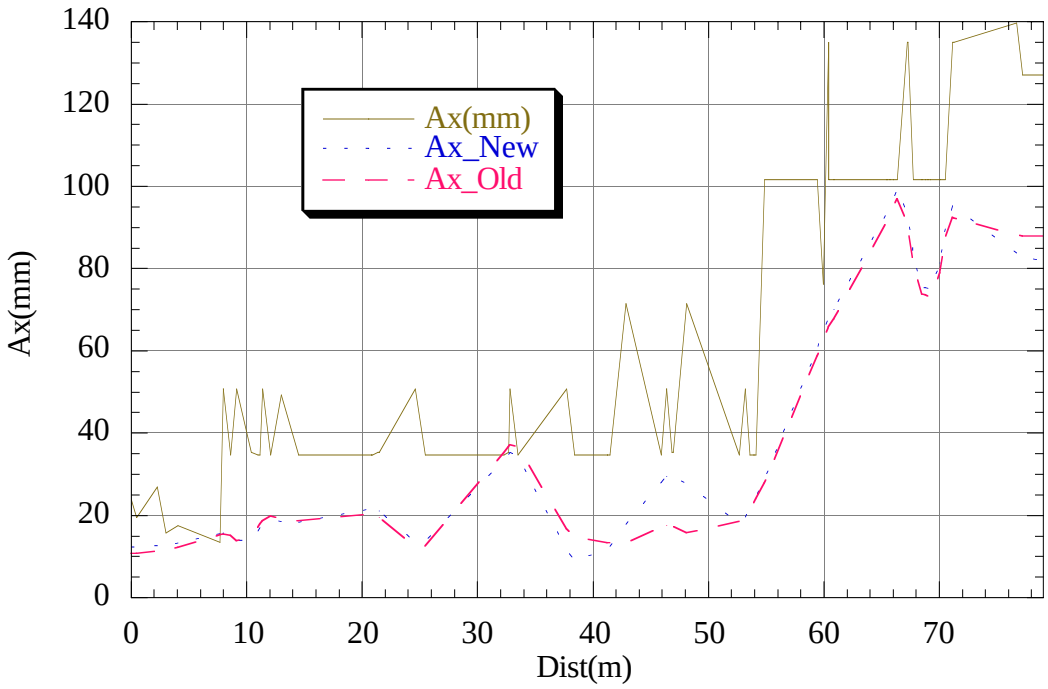

Figure 3.25. Horizontal aperture and beam envelope on the extraction orbit (Δp/p = .0086) in one sector (1/6th) of Accumulator; the formula used for the beam envelope is $A_x = \sqrt{\varepsilon\beta/\pi} + \left|D_x(\Delta p/p)\right|$ where ε = 15π mm-mrad (unnormalized)

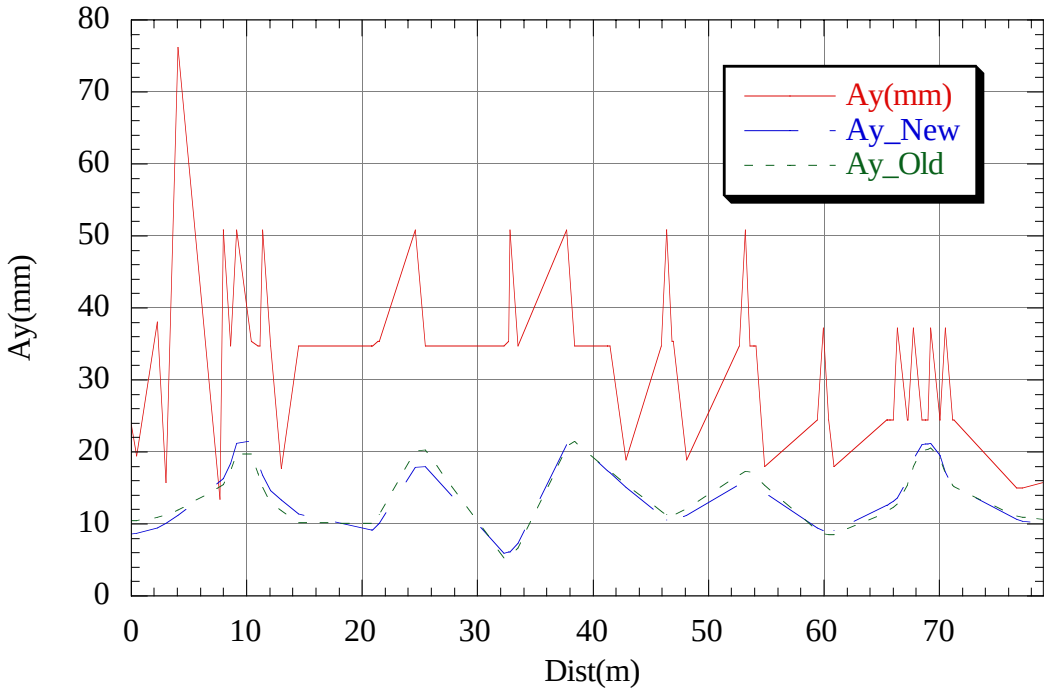

Figure 3.26. Vertical aperture and beam envelope on the central orbit in one sector (1/6th) of Accumulator; the formula used for the beam envelope is $A_y = \sqrt{\varepsilon\beta/\pi}$ where ε = 15π mm-mrad (unnormalized)

The phase advances from injection septum to kicker and from extraction kicker to extraction Lambertson magnet remain $3\pi/2$. The horizontal beta functions at the injection and extraction kickers will be slightly higher than they are now, so that the present kickers will be adequate in strength. Table 3.8 lists the lattice parameters at the injection septum and extraction Lambertson magnets for beam on the injection or extraction orbit. Small adjustments to the beam line quadrupoles can be made so that the beam lines are matched to the new Accumulator lattice at least as well as they are now.

Table 3.8. Lattice parameters at the injection septum and extraction Lambertson magnets.

Quantity	β_x(m)	β_y(m)	α_x	α_y	D_x(m)	D_x'	$\phi_x(2\pi)$
Septa and Lambertson (γ_τ=5.42)	15.77	7.58	0.55	0.02	0.30	0.10	0.21
Injection/Extraction Kickers (γ_τ=5.42)	11.44	13.46					1.01
Septa and Lambertson (γ_τ=6.58)	20.46	7.22	0.21	0.24	0.41	0.07	0.20
Injection/Extraction Kickers (γ_τ=6.58)	15.75	13.68					0.92

Nonlinear effects beyond those which can be corrected by families of sextupoles, octupoles, and skew quadrupoles are probably difficult to model with the magnetic field measurements that have been made to date. With the exception of the large β_x variation at Q10-Q11, the proposed lattice is very similar to that of the TEV I design, so that these effects will probably not change much. Figure 3.27 shows the measured tune variations across the momentum aperture with the extraction Lambertson magnet on. Turning the extraction Lambertson magnet off introduces a tune shift across the aperture, but does not change the basic shape of the tune vs. momentum plot. Introducing a local large orbit bump on the extraction orbit at any of the three high dispersion regions will produce a large tune shift. The Accumulator is operated with tunes decoupled on the core orbit, but the coupling is essentially 100% on the extraction orbit. A major portion of this coupling comes from the Lambertson magnet, and this coupling is a strong function of horizontal position in the Lambertson magnet. By design, the dispersion in the Lambertson magnet is 0.3 m, but the average measured dispersion is 0.8 m, and most of this arises between the extraction orbit and central orbit. In addition anomalous dispersion arises in all of the "zero dispersion" straight sections when the beam moves between the central orbit and the extraction orbit, making it impossible to optimize the aperture at all beam momenta. Figure 3.27 shows the measured orbit deviation between the core and extraction orbits, compared with the TEV I design. Beta function measurements at the core orbit and the central orbit agree well with each other and with the design; however beta function measurements at the extraction orbit deviate substantially from the design and have been difficult to interpret because of coupling.

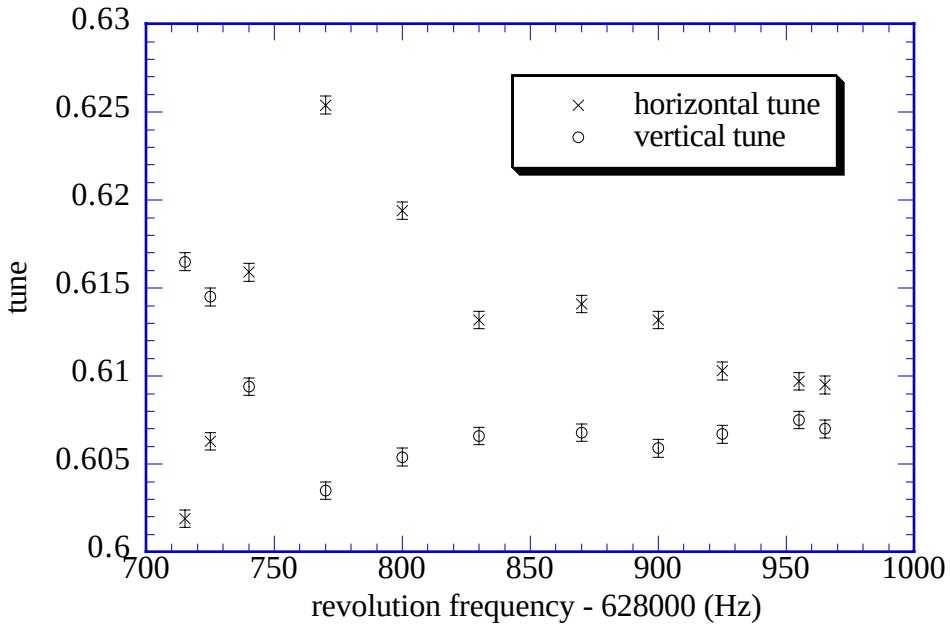

Figure 3.27. Measured Accumulator tune variations across the momentum aperture.

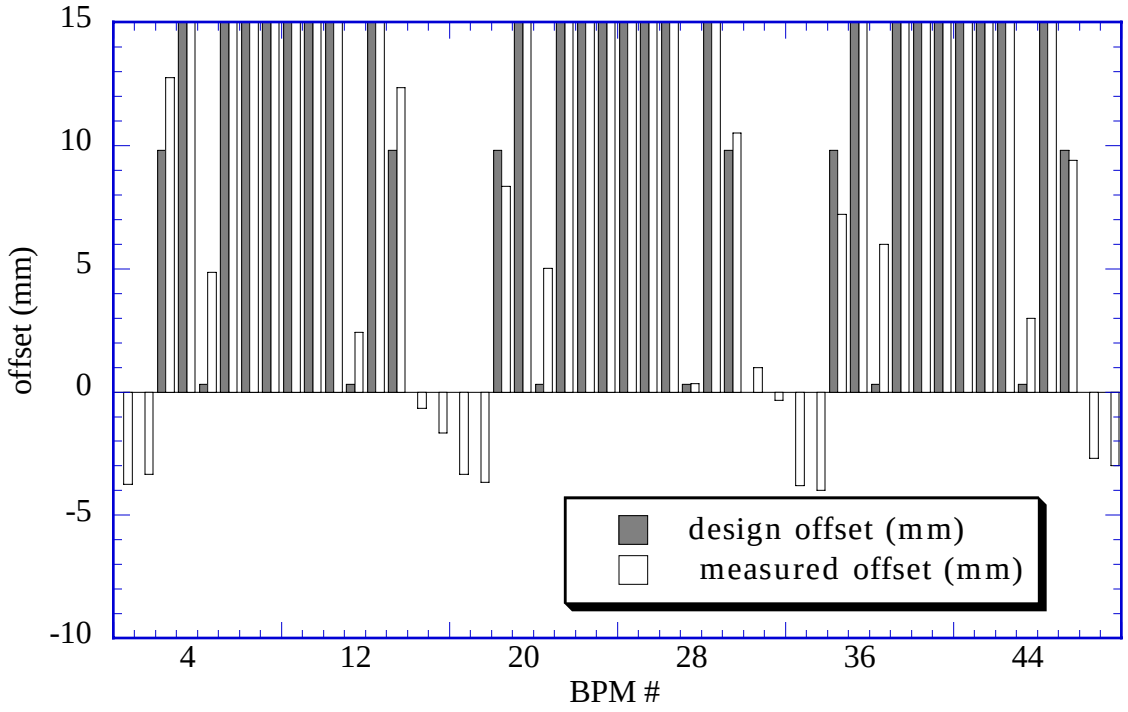

Figure 3.28. Measured and design Accumulator orbit difference between extraction orbit and core orbit on a scale showing dispersion error at the "zero dispersion" regions; high dispersion regions are off scale (about 140 mm).

It is known that some higher order resonances cause heating in the core – for example, the 8/13th (0.6154) and the 11/18th (0.6111). This is the motivation for choosing to run near the coupling resonance; it provides a large area in tune space free of higher order resonances. In addition, we currently operate with small negative chromaticities at the core, although there is no

strong evidence that operating at zero or slightly positive chromaticity at the core produces any instability.

3.4.3 Stack Tail Cooling System

The design of the 2-4 GHz stacktail system is based on scaling the TeV I 1-2 GHz stacktail design. The following quantities are scaled:

1. 1-2 GHz becomes 2-4 GHz
2. All beam energies stay the same
3. $\eta = 1/\gamma_t^2 - 1/\gamma^2$ becomes 0.012 (see section3.4.2)
4. The gain functions stay the same

With this scaling, the maximum flux is doubled. The power requirement is the same if the signal to noise ratio remains constant -- it should actually improve somewhat. Thus, rebuilding the stacktail system is essentially replacing the entire system part-for-part with higher frequency components. Some issues do need further investigation:

1. Fewer pickups are required to achieve the same signal to noise ratio. One might be able to achieve some savings in pickups.
2. The dependence of pickup sensitivity on transverse displacement was not what was expected for the 1-2 GHz system.
3. The Accumulator is designed to operate with the Recycler and to accumulate antiprotons for 1 to 4 hours. The optimum design for this type of operation might differ from a scaled TeV I design.
4. The effect on the stacking process of continual transfers from the Accumulator to the Recycler needs to be considered.

However, it is not foreseen that a better optimized design would differ dramatically in either cost or performance from the design that is simply scaled from TeV I.

The ultimate upgrade of the stacktail system could be to 4-8 GHz in the TeV33 era. This upgrade is not foreseen as being possible on the 1999 time scale. The design of the 4-8 GHz stack tail system would be radically different from either the 1-2 or 2-4 GHz systems, requiring frequent transfers to the Recycler Ring to take advantage of stacking capabilities of the electron cooling system. The lattice modification ($\eta = 0.012$) implemented for the 2-4 GHz system would also be appropriate for the 4-8 GHz system.

3.4.3.1 Design Considerations

Stochastic stacking is described in terms of the Fokker-Planck equation, which relates the time rate of change of the particle density to the initial density and the derivative of the density with respect to energy:

$$\frac{\partial \Psi}{\partial t} = \frac{\partial}{\partial E}\left[-F\Psi + \left(D_0 + D_1 + D_2\Psi\right)\frac{\partial \Psi}{\partial E}\right]$$

where $\Psi = \partial N/\partial E$ is the particle number density, F is the coefficient of the cooling term, the three D terms represent heating due to intrabeam scattering, thermal noise, and mixing. A complete derivation has been given by Möhl, et al..[20] A simplified steady state solution (ignoring for the moment thermal noise, mixing, and intrabeam scattering) results in an exponential density distribution, developed by an exponential voltage distribution. Our goal is to create an exponential

voltage distribution using beam pickups, amplifiers, electronic filters and phase compensation networks, and kicker electrodes. More complete details can be found in the TeV I Design report.[21]

As mentioned previously, the Run II stacktail system design is a scaling of the TeV I design to the frequency range of 2-4 GHz. The predicted pickup behavior as a function of beam position is an exponential falloff[22] as the particle moves far away from the center of the pickup. The pickup is placed in an area with large momentum dispersion (on the order of 8.5 m), correlating position with particle energy. With a symmetric lattice and non-zero value of η, there is a time difference in particle flight time between pickup and kicker as a function of energy. As the electronics time between pickup and kicker is fixed, the net phase of the voltage on the kicker changes with the particle energy. This phase slope leads to the use of multiple sets of pickups.

Three sets of pickups are used, two as the cooling inputs and two as compensation inputs (one set of pickups is used for both cooling and compensation). The compensation inputs are phased to null out the response in the region of the accumulated core. The first leg uses pickup set 1 as the cooling input and pickup set 2 as the compensation input. The peak response for leg 1 is centered in the vicinity where the input beam pulse is dropped off by the rf stacking. The second leg, which uses pickup set 2 as the cooling input and pickup set 3 as the compensation input, is positioned to best flatten the phase response. As the beam density is increasing as the beam energy decreases, there are fewer pickups required in sets 2 and 3 to attain a good signal to noise ratio.

3.4.3.2 Pickup Response Measurements

During the summer of 1997, a series of measurements was made using prototype 2-4 GHz pickups. These measurements were made in the Accumulator using antiprotons. Four different pickup designs were tested. A detailed account has been given by Derwent.[23] Figure 3.29 shows a comparison of the measured response and predicted response (with arbitrary normalization) as a function of the beam revolution frequency. The model response is normalized to the response of design #1. The measured response is in very good agreement with the predicted response.

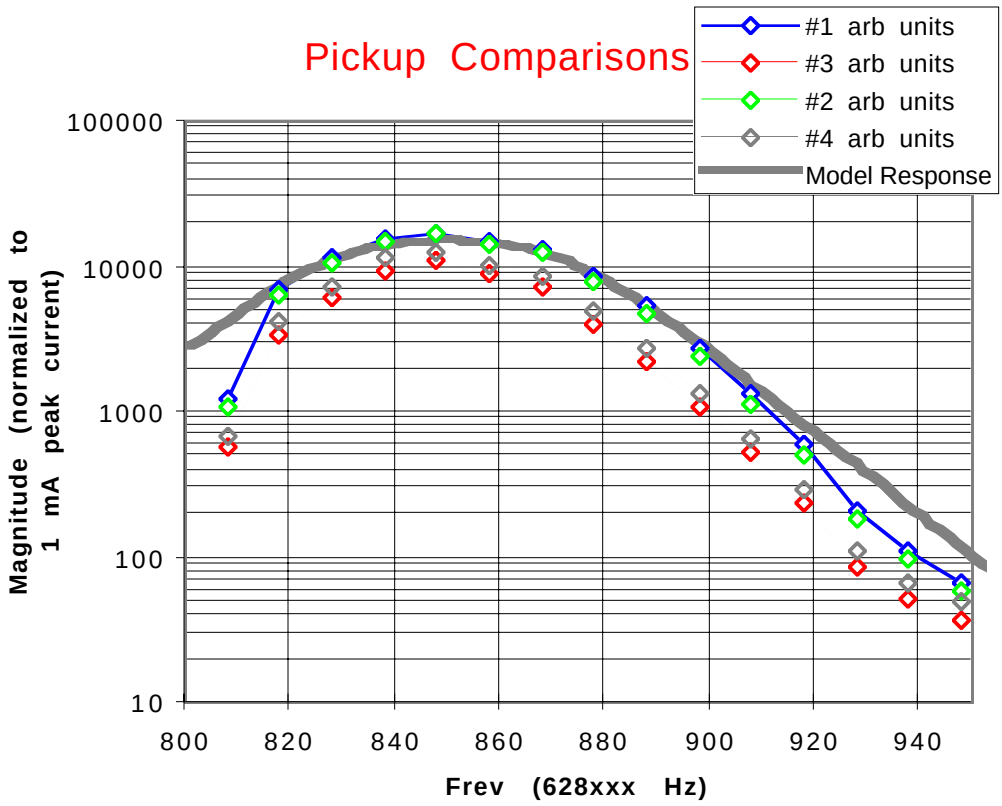

Figure 3.29. A comparison of measured and predicted pickup response

Of the four prototype pickup designs, two were similar to previous loop designs (#1 and #2) and two (#3 and #4) were designed to include phase compensation. By tilting the major axis of the pickup loop, thus changing the relative arrival time of the signal on the loop, it is possible to cancel some of the phase slope across the aperture. However, to keep the frequency response in the desired 2-4 GHz band, the pickup size became smaller. There is a tradeoff in the two designs -- better sensitivity (in #1 and #2) versus better phase behavior (#3 and #4). The impedance of the tilted loops is approximately 1/2 the impedance of the standard loops, requiring a factor of 2 in amplifier gain to get similar voltage response. This factor of two in amplifier gain results in a factor of four in noise power. As stacking simulations (discussed in the next section) achieve fairly uniform phase behavior using the standard loops, better pickup sensitivity has been chosen over better phase response.

3.4.3.3 Simulation Performance and Pickup Locations

The stacking simulation used in the system design is based on a simulation originally written by S. van der Meer for the CERN Antiproton Accumulator. The code does a numerical integration of the Fokker-Planck equation with a voltage gain function including the pickup response, amplification and electronic filtering, and kicker response. Beam feedback and thermal noise terms, which contribute to beam heating, are included. Further details can be found in reference.[24] The code has been modified to simulate the 2-4 GHz stacktail and the 4-8 GHz core cooling systems. At this time, it only simulates the longitudinal cooling and does not include any heating effects in the transverse plane.

The performance of the 1-2 GHz stacktail system, using the measured pickup response shapes as an input, has been simulated. With a minimum of optimization, the simulation predicts a stacking rate of 12 mA/hour, with an input flux of 18 mA/hour. Studies done with proton stacking

achieved a maximum rate of 12.2 mA/hour (see Ref. 1), well matched to the simulation results. This agreement gives confidence in the predictions of the simulation in extrapolating to the 2-4 GHz system.

The 2-4 GHz Accumulator stacktail system is assumed to have the following properties:

- $\eta = 1/\gamma_t^2 - 1/\gamma^2 = 0.012$
- Momentum Dispersion = 8.5 m at the pickup location
- Central Energy = 8.83 GeV
- Transverse aperture = 0.03 m at the pickup location
- Pickups and Amplifier are at 80 K physical temperature, with an amplifier noise temperature of 21 Kelvin (0.3 dB noise figure)
- Pulses are injected every 1.5 seconds
- RF stacking deposits 1e8 particles per pulse at an energy of +14 MeV with respect to the central energy and with a half width of 7.8 MeV

These assumptions give a maximum stacking rate of 24 mA/hour.

In Figure 3.30 we show the calculated gain response for the choice of the pickup positions. Pickup set 1 is at an energy of 15.3 MeV (a position of 14.7 mm from the central orbit), pickup set 2 is at an energy of -3.8 MeV (-3.7 mm), and pickup set 3 is at an energy of -22.9 MeV (-22.0 mm). The phase of the system (desire 180˚ between 20 MeV and -60 MeV) is shown in Figure 3.31. The phase stays within 30˚ of the desired value, and the magnitude of the response varies only 15% from optimum.

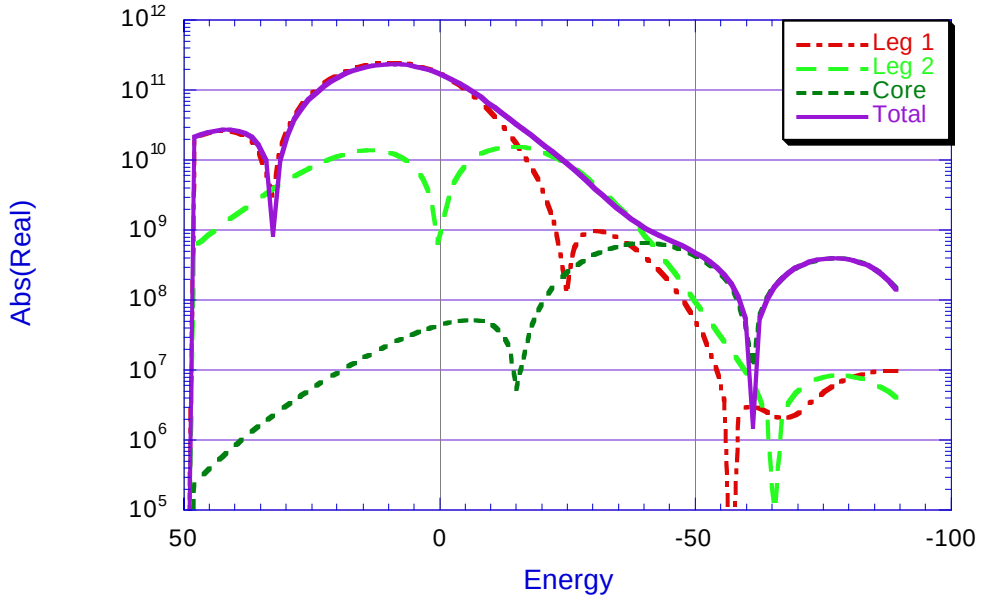

Figure 3.30. The absolute value of the real part of the system gain. The dips indicate where the gain changes sign (from cooling to heating).

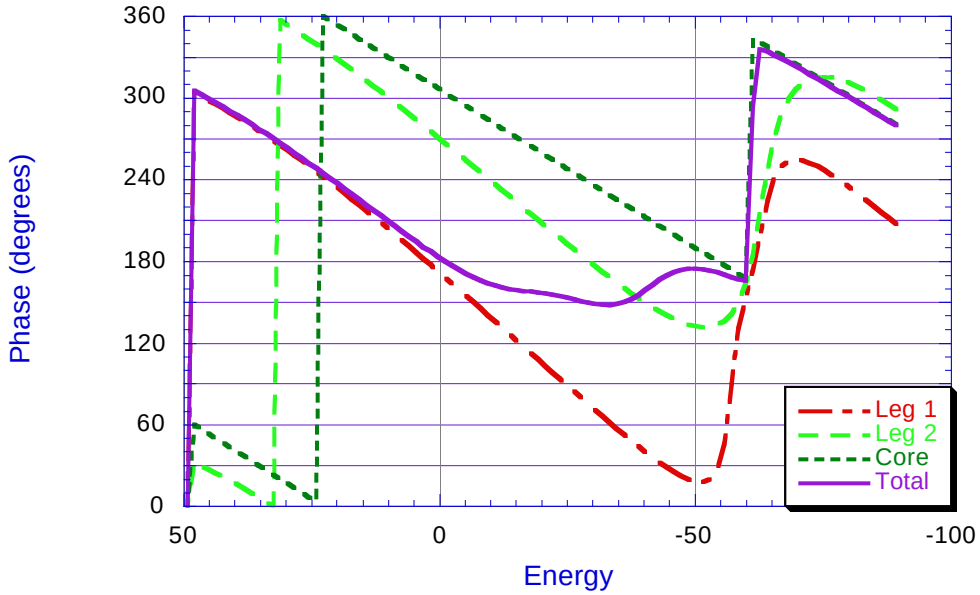

Figure 3.31 The Phase of the stacktail system. A phase of 180˚ is desired from 20 MeV to -60 MeV.

Simulations have been run for three hours of stacking with this system, putting in 1×10^{8} antiprotons every 1.5 seconds. Figure 3.32 shows the energy density distribution, with one curve every 30 minutes of stacking. The core is evident after the first half hour. The effects of extraction to the Recycler have not been simulated.

Figure 3.33 shows the stack size (in mA) and stack rate (in mA/hour) over the three hour time period simulated. The stack rate is equivalent to the injected flux for approximately the first 90 minutes and then it begins to drop off slowly, going down to 22 mA/hour after 3 hours. Over the 3 hour time period, 70.5 mA are accumulated, an average of 23.5 mA/hour.

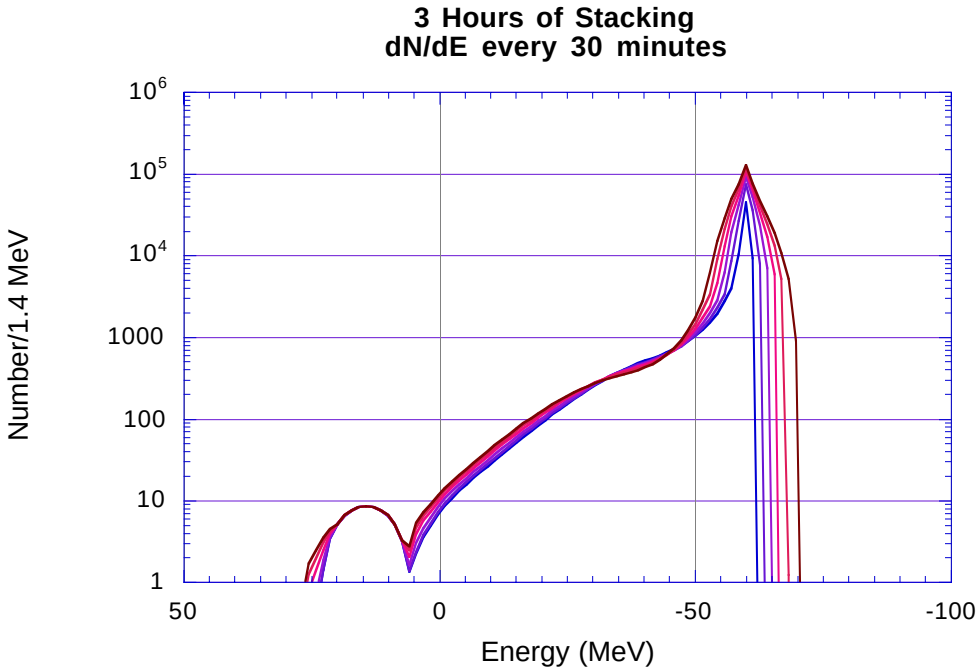

Figure 3.32. The stack density distribution for 3 hours of stacking, showing the distribution every 30 minutes. The bump on the left is the injected beam.

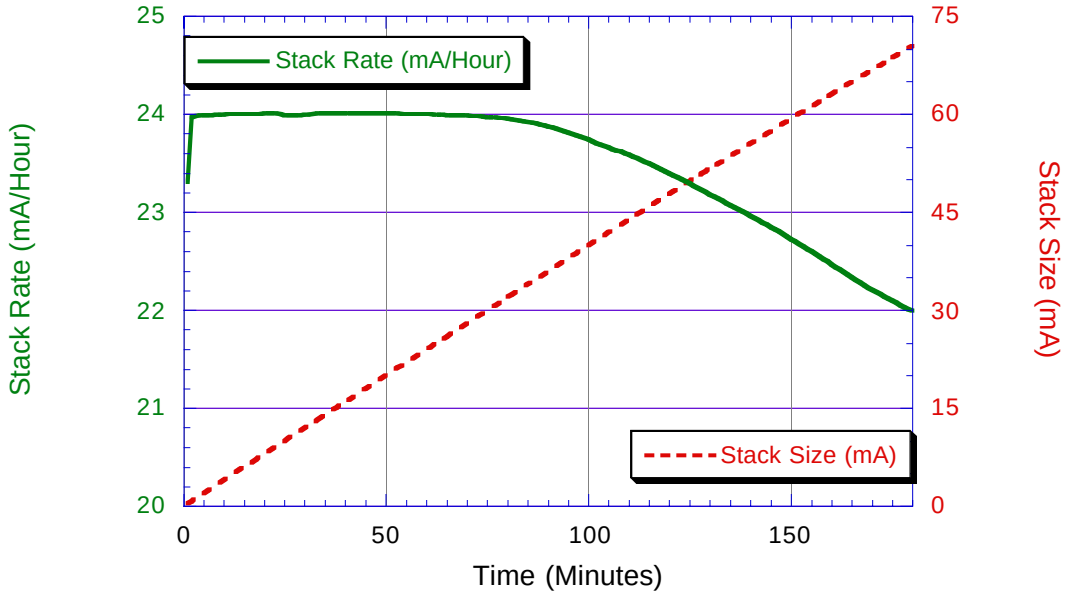

Figure 3.33. The stack rate (solid and left axis) and stack size (dashed and right axis) for the nominal configuration. 24 mA/hour are injected into the system. An average of 23.5 mA/hour over the three hours simulated is achieved.

3.4.3.4 Signal to Noise Ratio and Power

As the system uses high gain amplifiers, the dominant noise component for the signal to noise ratio calculation is the noise coming from the front-end amplifier. With 2 GHz of bandwidth and 80 ˚K temperature, the noise power is -86.3 dBm. The signal power is calculated using the measured impedance of the 16 loop combiner boards, multiplied by the number of combiner boards, and convoluted with the number density distribution from the stacking simulations. With 16 arrays at 15.3 MeV, the signal power is -80.8 dBm; 4 arrays at -3.8 MeV contribute -80.2 dBm. There is adequate signal to noise for the system in this configuration. The system design described in the previous section uses slightly more than 500 watts of power after two hours of stacking, with 90 watts of the total in noise power.

3.4.3.5 Design Sensitivity

The performance of the stacktail system is dependent upon the momentum dispersion (since the pickup sensitivity depends upon the position displacement) and pickup positions. Simulation runs have been done with variations in the dispersion and pickup position to quantify the sensitivity.

Two hour stacking simulations have been run with dispersion values of 8.1 m, 8.5 m, and 8.9 m. The pickups have been kept at the same physical location with respect to the central orbit (at 14.7, -3.7, and -22 mm respectively). The electronic phase and gain settings were not changed. Over the 2 hour time period, the stacking rate for the 3 scenarios varied by less than 1%. We conclude that small variations in the dispersion around the design goal of 8.5 m should not be a significant problem.

The phase hand-off between leg 1 and leg 2 depends upon the relative position, gain, and phase of the two legs. Displacement of the legs with respect to the beam can change the system performance. For example, assume that the central orbit is not centered through the pickup tanks. A coherent shift of the three pickup sets is used to simulate this possibility. Alignment errors can be simulated by moving the pickup sets independently. Both scenarios have been tested over a ±10 mm range of displacement. Figure 3.35 shows the results of these simulations. Displacements within ±5 mm of the nominal positions, in either leg or both legs, lead to small changes in the stacking rate. The stacking rate falls by factors of 1.1 to 3 when the displacements are extended to ±10 mm.

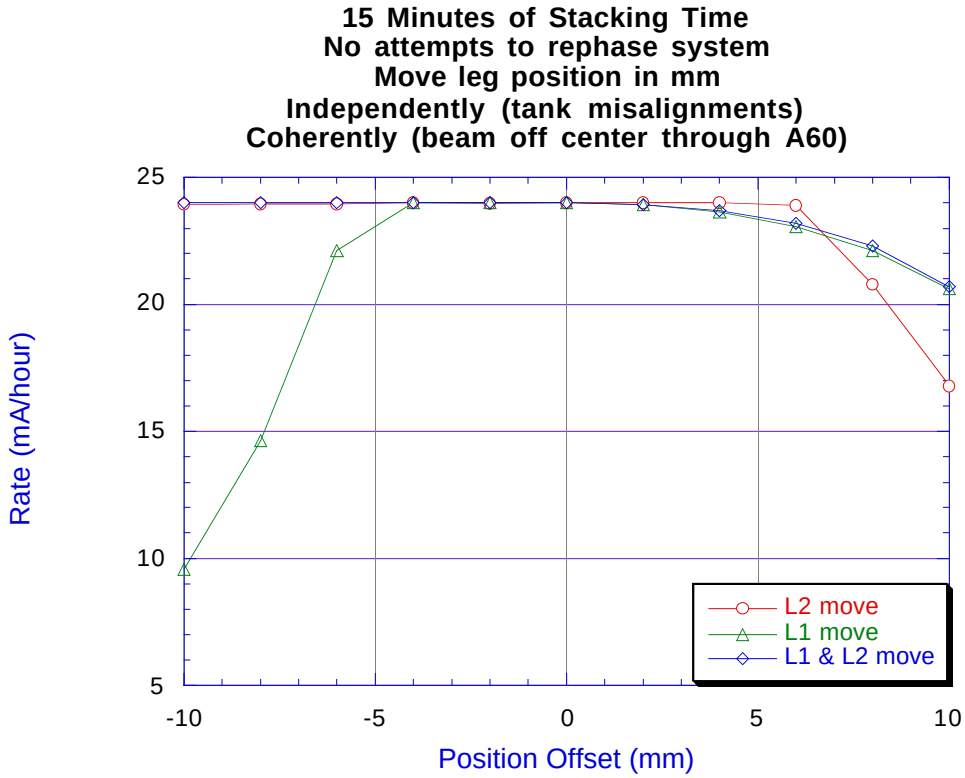

Figure 3.35. The stacking rate as the position of the pickup sets is moved relative to the nominal position. The open circles are moving Leg 2, keeping Leg 1 in the nominal position, the triangles are moving Leg 1, keeping Leg 2 in the nominal position, and the diamonds are moving Legs 1 and 2 together.

3.4.4 Core cooling systems

3.4.4.1 Core cooling requirements

The core cooling systems are required to provide a transverse beam size of 10π mm-mrad for transfer to the Recycler. The time allotted to achieve this emittance is 5% of the stacking time or about 5 to 10 minutes. Figure 3.36 shows the core transverse emittance during stacking as a function of stack size in Run Ib. At a stack size of 100×10^{10} the emittance is 0.6π to 1.0π mm-mrad (6π to 10π mm-mrad normalized), which meets the Recycler criterion immediately after stacking is turned off. However, the transverse cooling rate will decrease because of the factor of about 2 increase in the mixing parameter. This fact should result in a factor of two reduction in cooling rate, but it does not because the core cooling system operates well below the optimum gain. While Figure 3.36 provides a guide, there is no assurance that the transverse heating of the new stack tail system will be the same as the old system (it could be better or worse depending on construction details).

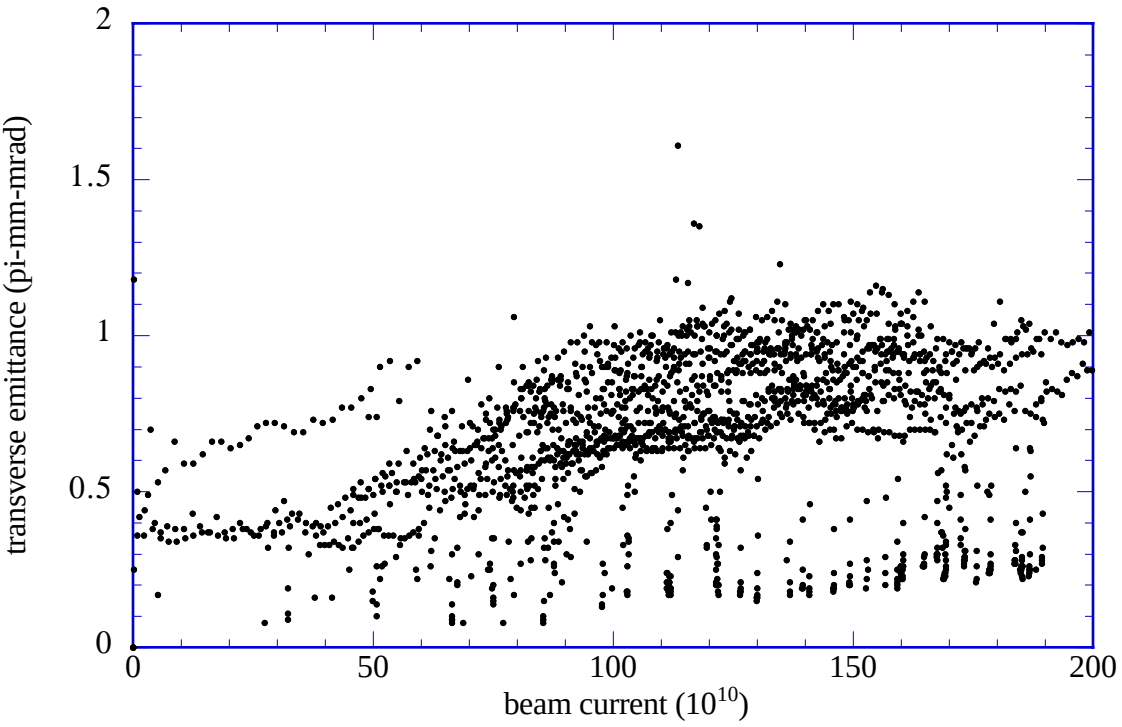

Figure 3.36. Transverse emittance vs. stack size during stacking

There is no specific requirement on the longitudinal density of the beam. We do not expect to be able to capture 100% of the beam longitudinally in a 10 eV-sec phase space. Our experience is that for a fixed longitudinal phase space, more beam can be extracted with a larger stack than a smaller one, but that the fraction of the stack that can be extracted decreases monotonically with stack size. If, for example, we start with a stack of 50×10^{10} antiprotons and we stack an additional 50×10^{10} antiprotons , then we must be able to capture 50% of the beam in order to return to the initial condition. The increase in the amount of beam captured with larger stacks, however, must be balanced against the larger transverse emittance and the frequency and duration of transfers required in order to maximize the efficiency of transfer to the Recycler.

During the course of Run 1b a variety of RF bucket areas were used for unstacking 6 antiproton bunches, but the total longitudinal phase space area was always 10 eV-sec or less.[25] The fraction of the antiproton stack extracted as a function of stack size for each size rf bucket is shown in Figure 3.37. Figure 3.37 shows that the fraction of the antiproton stack which is removed during the course of unstacking decreases with increasing stack size. At an intensity of $100\text{x}10^{10}$ antiprotons it is possible to remove 50 to 60% of the antiproton stack . However, these results were obtained long after the stack tail system had been turned off and we expect at least a modest decrease in cooling rate because of the increase in the mixing factor. The stack size, the longitudinal emittance, and the transfer frequency will all be optimized operationally in order to accumulate antiprotons at the maximum rate in the Recycler.

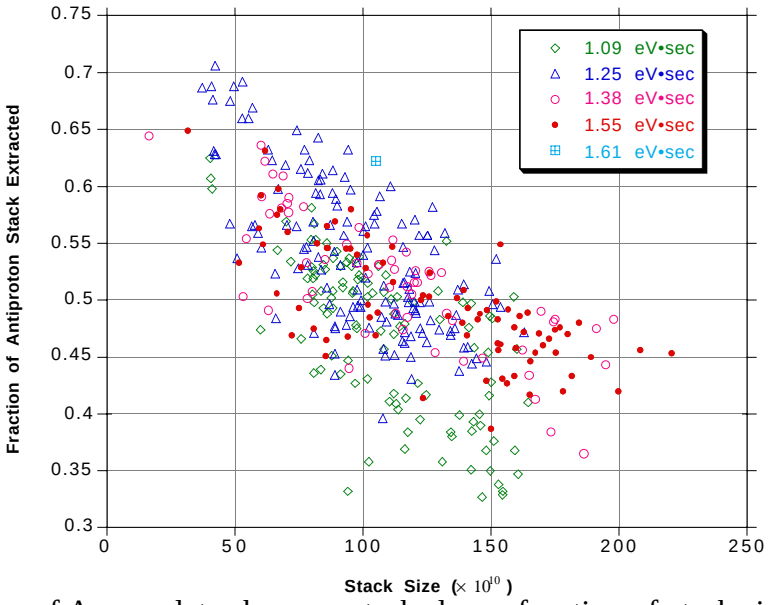

Figure 3.37. Fraction of Accumulator beam unstacked as a function of stack size for different RF buckets. Note the suppressed zero on the vertical axis.

3.4.4.2 Performance of the current 4-8 GHz systems

The currently installed core cooling systems are characterized by low gain (compared to the optimum gain) at the low end of the frequency band and even lower gain at the high frequency end. A measurement of signal suppression is shown in Figure 3.38. The measurement shows perhaps 1 dB of signal suppression (12% of the optimum gain) at 4.5 GHz. A measurement of the transfer function is shown in Figure 3.39. The system gain drops about 15 dB from 4 to 8 GHz. We believe that the gain can be substantially increased by improving the pickup response and improving the method of signal transmission across the ring.

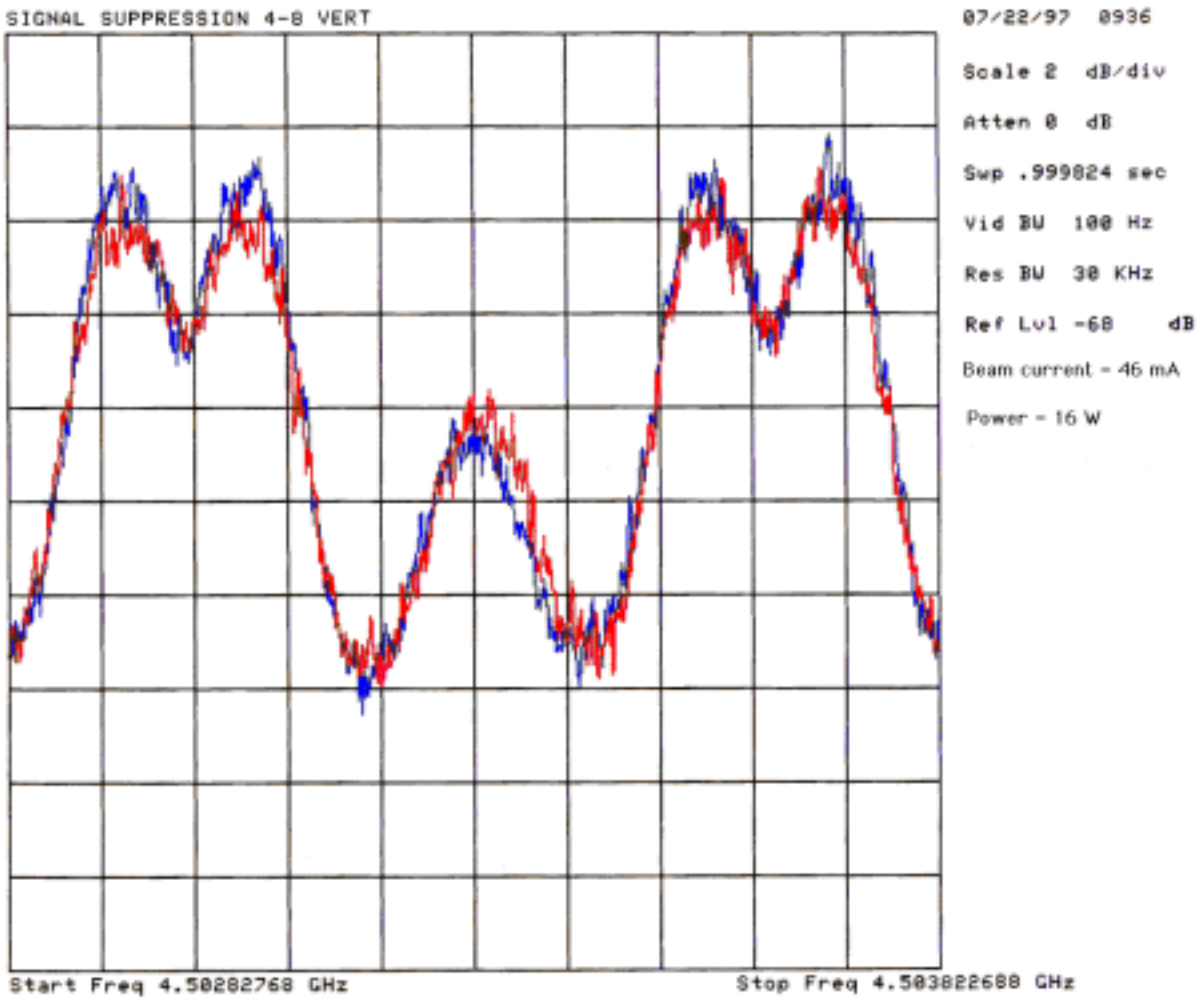

Figure 3.38. Signal Suppression measurement on the 4-8 GHz Core Vertical Cooling system.

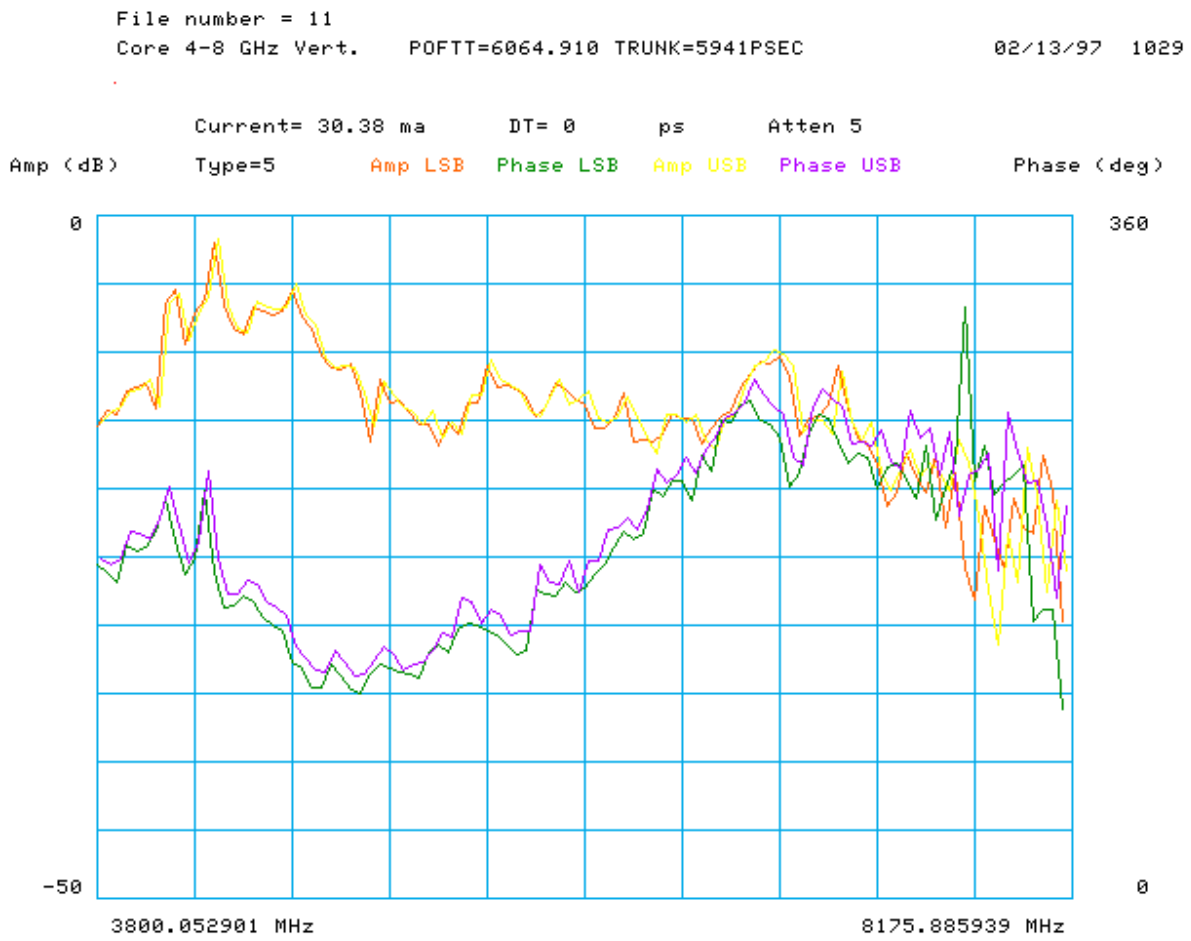

Figure 3.39. Transfer function measurement of the 4-8 GHz core cooling system.

3.4.4.3 Core cooling pickups and kickers

The core cooling pickups and kickers do not have a uniform response in the 4-8 GHz range. The measured signal to noise ratio of the sum mode from the core vertical PU is shown in Figure 3.40. The amplifier noise power is nearly independent of frequency, so the data indicate a decrease in sensitivity of about 10 dB over the frequency range. The non-uniform response makes it difficult to achieve the full cooling bandwidth of 4 GHz. The problem is particularly severe in the kickers which have an additional 1/f factor in the frequency response of the transverse kick applied to the beam.

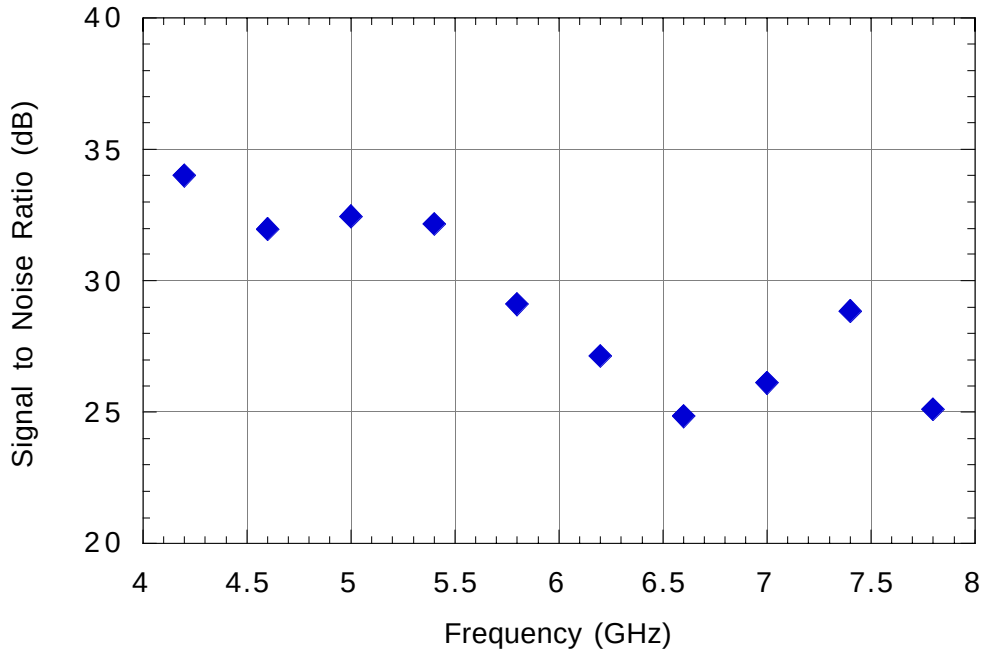

Figure 3.40. Signal to noise ratio measurement of the 4-8 GHz Vertical Core Cooling system.

We do not have a specific proposal for improving the frequency response of the 4-8 GHz pickups. However, our work with the Debuncher prototypes shows that high sensitivity can be achieved in this frequency range subject to the requirements of cost and space in the lattice. We intend to develop a practical plan when the design work of the stack tail cooling system is more advanced. The goal will be to increase the sensitivity at the low frequency end by 3 dB and to produce a pickup response that is flat to within 5 dB over the 4-8 GHz band.

3.4.4.4 Transmission of the 4-8 GHz signals

Aside from the pickup and kicker response, the most serious problem in shaping the gain of the 4-8 GHz cooling system is the transmission of the signal across the ring. The cable used for this purpose has a variation in attenuation across the 4-8 GHz band of about 10 dB. While it is possible to compensate this loss with equalizing filters, the equalization achieved is less than perfect. The measured gain of the electronics is shown in Figure 3.41 and shows a generally rising gain with frequency. However, it is clear from the sloping gain function (see Figure 3.39) that the equalization is far from perfect.

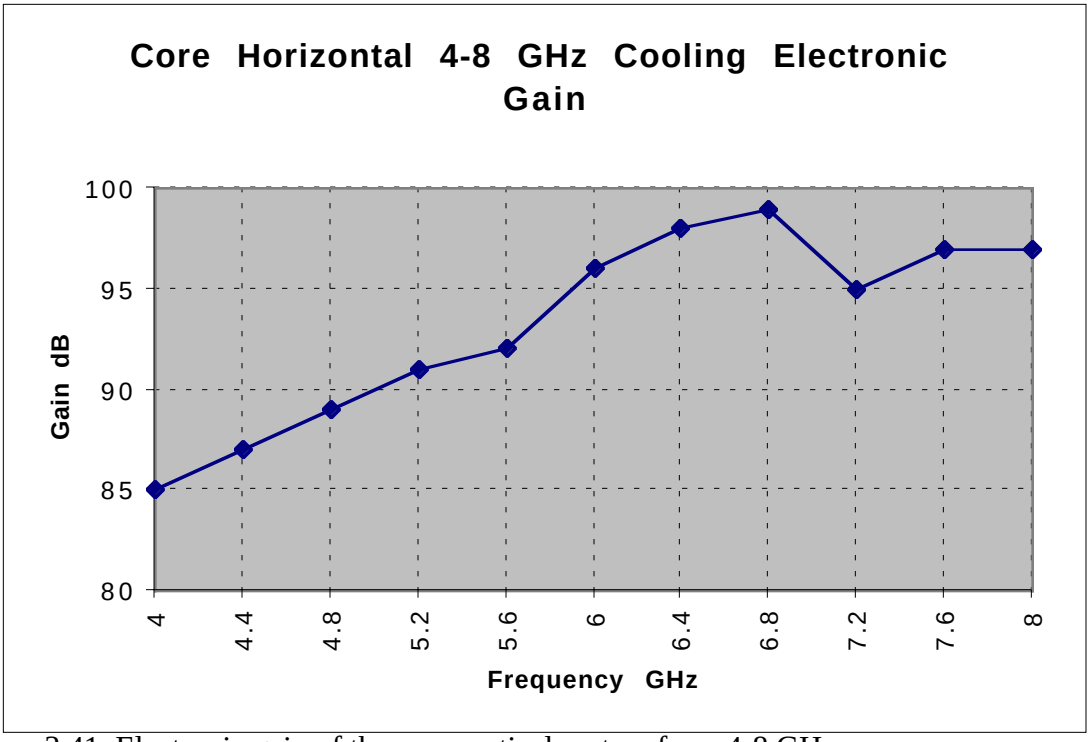

Figure 3.41. Electronic gain of the core vertical system from 4-8 GHz.

A R&D program was started in February 1996 to study the possibility of transmitting microwave signals using free space laser optical techniques. Initial calculations show that signal transmission is indeed possible over distances of hundreds to thousands of feet. This technique will reduce the severity of the equalization problem in the Accumulator and is essential for the Recycler stochastic cooling systems.

Wide band microwave optical transmission has been in use at Fermilab since the late 1980's. Signal bandwidths exceeding 12 GHz have been transmitted over 6 kilometers of single mode fiber with flat gain and phase response, plus minus 2 dB and 15 degrees of phase. The penalty of using fiber optic transmission links is a nominal 35-40 dB insertion loss due to matching networks between the microwave source/termination and the low impedance laser diode and pin photo diode. The insertion loss of the single mode fiber is on the order of 0.2 dB/kilometer and does not effect system performance for the delays associated with systems at Fermilab. Another consideration of optical transmission techniques is the dynamic range requirement. The development of Distributed Feedback Laser diodes, DFB, has increased the dynamic range of laser systems by providing a monochromatic laser source that also suffers less from the dispersion of the fiber optic waveguide. Dynamic range in excess of 40 dB is obtainable over moderate microwave bandwidths.

Unfortunately, the velocity of propagation on single mode fiber is approximately 67% that of light in free space. This slow propagation makes it impossible to send stochastic cooling signals across the ring in time synchrony with the beam. A solution utilizing free space propagation would solve this problem. Externally modulated lasers do not have octave microwave modulation bandwidths. Solid state lasers are the only available source of wideband analog optical transmission. Testing of free space optical transmission using fiber optic based optical transmission links was started in February of 1996. A test at the A0 test facility with the help of the University of Rochester graduate students showed that a series of beam expanding telescopes could be successfully employed to make the fiber to free space transition. The early test utilized components that were not properly coated for the 1310 nanometer wavelength of the optical system. Nonetheless successful transmission was made on a light table with acceptable results for

stochastic cooling systems. Based on this early success, procurement of catalog optical devices with the proper wavelength coating was initiated. The fiber to free space expanders and telescopes were received in the summer of 1996. The bench test of the new optics proved to have 10 times less insertion loss than the original bench test from February.

Mechanical stability proved to be the next obstacle. The core of the single mode fiber is 9 microns in diameter making alignment very sensitive to temperature variations and microphonics. The alignment stability of the system can be measured in minutes, so some type of feed back is required. Fortunately, our system is not the first to suffer from this problem and catalog hardware is available to remedy the alignment instability.

An additional requirement is that the free space propagation medium have an extremely stable index of refraction, on the order of ten parts per million. This specification is dictated by the 5-20 picosecond delay stability required for 4-8 GHz bandwidth cooling. The only conceivable means of providing such a stable medium is the use of an evacuated pipe with end windows that are transparent at 1310 nanometers. This requires some conventional construction for the placement of optically flat pipes buried at the tunnel ceiling level. (There is insufficient time of flight in the accumulator systems to come to the surface.)

A prototype system has been built, installed in the Accumulator 4-8 GHz cooling systems, and tested in the summer of 1997. The optical system was installed as a parallel path so that it could be tested concurrently with normal operations. The gain was measured to be flat within ±2 dB. The optical system behaved as expected, but requires equalization before becoming operational. We plan to design the equalization when the new pickup and kicker assemblies are installed.

3.5 Unstacking Scenario

The scenario we propose for extracting antiprotons from the Accumulator to the Recycler uses only the 2.5 MHz H=4 rf system. The frequency of transfers will be determined based on experience, but in this section we assume transfers about every two hours. When the Accumulator stack reaches 60×10^{10} antiprotons into the core, the injection of new beam pulses will be interrupted and the core will be immediately adiabatically bunched with the H=4 RF system. The 2.5 MHz voltage will be raised adiabatically to about 250 Volts corresponding to a total bucket Area of 10 eV-sec in order to capture about 40×10^{10} antiprotons. The four bunches will be accelerated across the aperture with a synchronous phase angle of 5° while the voltage keeps increasing to 450 Volts. At the extraction orbit the bucket area will be about 3.7 eV-sec while the longitudinal emittance of each bunch will be around 2.5 eV-sec. The beam in each bunch will occupy about 240 nsec out of 400 nsec leaving about 160 nsec for the extraction kicker rise time.

At this point the antiprotons will be transferred bucket to bucket to the Recycler Ring. The Recycler low level rf RRRF has opened a beam gap and has cogged the Recycler aa marker (RRaa) to the gap.

The Accumulator synchronizes to the Recycler aa marker (RRaa) at the Recycler Revolution frequency Frr and the MILLRF and MIBS will also synchronize to Frr and RRaa. The required Recycler voltage for a synchronous bucket to bucket transfer is 2.3 kV.

Following transfer, the Accumulator will recommence stacking with an initial stack consisting of the remaining 20×10^{10} antiprotons. Assuming a stacking rate of 20×10^{10} antiprotons per hour transfers will occur every 2 hr.

---

[1] With a 5 sec main ring repetition rate. A stacking rate of $9.7\text{x}10^{10}$/hour was achieved with a 2.4 sec repetition rate. See M. Church, Pbar Note 560 (unpublished) for more details.

[2] F. M. Bieniosek, K. Anderson and K. Fullett, Proc. 1995 US Particle Accelerator Conference. F. M. Bieniosek, Fermilab-TM-1857 (1993).

[3]C. M. Bhat and N. V. Mokhov, Fermilab-TM-1585 (1989).
[4]S. O'Day and F. M. Bieniosek, Proc. 1993 US Particle Accelerator Conference, p.3096.
[5]F. M. Bieniosek and K. Anderson, Proc. 1993 US Particle Accelerator Conference, p. 3163.
[6]G. Dugan et al., IEEE Trans. Nucl. Sci.30:3660-3662(1983).
[7]S. O'Day and K. Anderson, Proc. 1995 US Particle Accelerator Conference,
[8]F. M. Bieniosek, pbar Note #550 (1994).
[9]Fermilab. *Design Report for Tevatron I Project.* Batavia, Illinois: Fermi Natl. Accel. Lab (1984)
[10]Mohl D. *CERN Internal Rep. CERN 87-03* V2:453-533 (1987)
[11]Bisognano J, Leeman C. AIP Conf. Proc. #87, Fermilab Summer School on Acc. Physics (1981)
[12] D. McGinnis, Pbar Note No. 564 (unpublished). See also the world wide web at http://131.225.123.174/DaveMc/debuncher_upgrade/debunch.htm.
[13] D. McGinnis, Pbar Notes No. 564 and 565 (unpublished) and the World-Wide-Web, *loc. cit.*
[14] ACOL reference
[15] PU calculation
[16] Dave McGinnis, pbar note xxx.
[17] Do we have a reference?
[18]Bisognano J, Leeman C. *AIP Conf. Proc. #87, Fermilab Summer School on Acc. Physics* (1981)
[19]Fermilab, *Design Report for Tevatron I Project* (1984).
[20] D. Möhl, G. Petrucci, L. Thorndahl, and S. van der Meer, Physics Reports C, 58 (1980) 73-119.
[21] Design Report Tevatron I Project, Fermi National Accelerator Laboratory, September 1984.
[22] A.G. Ruggiero, "Pickup Loop Analysis" Pbar Note 148 (1981), unpublished; A.G. Ruggiero, "More Analysis of Pickups (Strip Lines) Sum and Difference Modes Dependence on Vertical Displacement", Pbar Note 199 (1982), unpublished.
[23] P.F. Derwent, "Stacktail Prototype Pickups", http://www-bd.fnal.gov/ap/documents/upgrades/prototype.html (1997), unpublished.
[24] John Marriner and Vladimir Visnjic, "Fermilab Stochastic Cooling Code User's Guide", Pbar Note 498 (1991), unpublished.
[25] The text of this paragraph and Figure 3.37 were adapted from V. Bharadwaj, et al., TM-1970.